NASA TECHNICAL MEMORANDUM 107676

ADVANCES IN FATIGUE LIFE PREDICTION METHODOLOGY FOR METALLIC MATERIALS

J. C. Newman, Jr.

AUGUST 1992

National Aeronautics and Space Administration

Langley Research Center
Hampton, Virginia 23665-5225

ADVANCES IN FATIGUE LIFE PREDICTION METHODOLOGY FOR METALLIC MATERIALS

J.C. Newman, Jr.
NASA Langley Research Center
Hampton, Virginia

ABSTRACT

The objective of this paper is to review capabilities of a plasticity-induced crack-closure model to predict small- and large-crack growth rates, and in some cases total fatigue life, for four aluminum alloys and three titanium alloys under constant-amplitude, variable-amplitude, and spectrum loading. Equations to calculate a cyclic-plastic-zone corrected effective stress-intensity factor range from a cyclic J-integral and crack-closure analysis of large cracks were reviewed. The effective stress-intensity factor range against crack growth rate relations were used in the closure model to predict small- and large-crack growth under variable-amplitude and spectrum loading. Using the closure model and microstructural features, a total fatigue life prediction method is demonstrated for three aluminum alloys under various load histories.

NOMENCLATURE

A_i	Coefficients in crack-opening stress equation
a	Crack length measured in thickness (B) direction, mm
a_i	Initial crack length measured in thickness direction, mm
B	Specimen thickness, mm
c	Crack length measured in width (w) direction, mm
c_i	Initial crack length measured in width direction, mm
d	Crack length plus portion of cyclic-plastic-zone size, mm
F_j	Boundary correction factor on stress-intensity factor

K_{max}	Maximum stress-intensity factor, MPa-$\sqrt{m}$
K_{OL}	Overload stress-intensity factor, MPa-$\sqrt{m}$
K_{UL}	Underload stress-intensity factor, MPa-$\sqrt{m}$
N	Number of cycles
N_f	Number of cycles to failure
N_p	Predicted number of cycles to failure
N_t	Number of cycles to failure in test
R	Stress ratio (S_{min}/S_{max})
r	Notch or hole radius, mm
S	Applied stress, MPa
S_o	Crack-opening stress, MPa
S_o'	Crack-opening stress for extreme crack-growth rates, MPa
S_{max}	Maximum applied stress, MPa
S_{mf}	Mean flight stress, MPa
S_{min}	Minimum applied stress, MPa
t	Specimen thickness for through crack or corner crack and specimen half-thickness for surface crack, mm
w	Specimen half-width, mm
α	Constraint factor on tensile yielding around crack front
Δc	Crack extension in c-direction, mm
ΔK	Stress-intensity factor range, MPa-$\sqrt{m}$
ΔK_{eff}	Effective stress-intensity factor range, MPa-$\sqrt{m}$
$\Delta \bar{K}_{eff}$	Cyclic plastic zone corrected effective stress-intensity factor range, MPa-$\sqrt{m}$
$(\Delta K_{eff})_{th}$	Small crack ΔK_{eff} threshold, MPa-$\sqrt{m}$
ΔK_{th}	Large-crack stress-intensity factor range threshold, MPa-$\sqrt{m}$
ρ	Plastic-zone size, mm

σ_o	Flow stress (average between σ_{ys} and σ_u), MPa
σ_{ys}	Yield stress (0.2 percent offset), MPa
σ_u	Ultimate tensile strength, MPa
ω	Cyclic-plastic-zone size, mm

INTRODUCTION

The use of damage-tolerance concepts, and to some extent durability, to predict fatigue-crack-growth lives in aircraft structures is well established [1,2]. The safe-life approach, using standard fatigue analyses, is also used in many designs. In conventional metallic materials, crack-growth anomalies such as the small-crack effect and the various crack-tip shielding mechanisms [3,4] have improved our understanding of the crack-growth process but have complicated life-prediction methods. In the new metallic materials, such as the aluminum-lithium alloys, crack growth, crack shielding and failure mechanisms are more complex than in conventional materials due to crack growth along tortuous crack paths [5]. Over the past decade, the intense experimental studies on small or short crack growth behavior in these metallic materials have led to the realization that fatigue life of many engineering materials is primarily "crack propagation" from microstructural features, such as inclusion particles, voids or slip-band formation. Concurrently, the improved fracture-mechanics analyses of some of the crack-tip shielding mechanisms, such as plasticity- and roughness-induced crack closure, and analyses of surface- or corner-crack configurations have led to more accurate crack growth and fatigue life prediction methods.

On the basis of linear-elastic fracture mechanics (LEFM), research studies on small cracks (10 μm to 1 mm) have shown that small cracks grow much faster than would be predicted from large crack data [3,4]. This

behavior is illustrated in Figure 1, where the crack-growth rate, da/dN or dc/dN, is plotted against the linear-elastic stress-intensity factor range, ΔK. The solid (sigmoidal) curve shows typical results for large cracks in a given material and environment under constant-amplitude loading ($R = S_{min}/S_{max}$ = constant). The solid curve is usually obtained from tests with large cracks. At low growth rates, the threshold stress-intensity factor range, ΔK_{th}, is usually obtained from load-reduction (ΔK-decreasing) tests. Some typical results for small cracks in plates and at notches are shown by the dashed curves. These results show that small cracks grow at ΔK levels below the large-crack threshold and that they also can grow faster than large cracks at the same ΔK level above threshold. Small-crack effects have been shown to be more prevalent in tests which have compressive loads, such as negative stress ratios [6,7].

During the last decade, research on the small- or short-crack effects has concentrated on three possible explanations for the behavior of such cracks. They are plasticity effects, metallurgical effects and crack closure [3,4]. All of these features contribute to an inadequacy of linear-elastic fracture mechanics (LEFM) and the use of the ΔK-concept to correlate fatigue crack growth rates.

Some of the earliest small-crack experiments were conducted at high stress levels which were expected to invalidate LEFM methods. Nonlinear or elastic-plastic fracture mechanics concepts, such as the J-integral and an empirical length parameter [8], were developed to explain the observed small-crack effects. Recent research on the use of ΔJ as a crack-driving parameter suggest that plasticity effects are small for many of the early and more recent small-crack experiments [9]. But the influence of plasticity on small-crack growth and the appropriate crack-driving parameter is still being debated.

Small cracks tend to initiate in metallic materials at inclusion particles or voids, in regions of intense slip, or at weak interfaces and grains. In these cases, metallurgical similitude [3,4,10] breaks down for these cracks (which means that the growth rate is no longer an average taken over many grains). Thus, the local growth behavior is controlled by metallurgical features. If the material is markedly anisotropic (differences in modulus and yield stress in different crystallographic directions), the local grain orientation will strongly influence the rate of growth. Crack front irregularities and small particles or inclusions affect the local stresses and, therefore, the crack growth response. In the case of large cracks (which have large fronts), all of these metallurgical effects are averaged over many grains, except in very coarse-grained materials. LEFM and nonlinear fracture mechanics concepts are only beginning to explore the influence of metallurgical features on stress-intensity factors, strain-energy densities, J-integrals and other crack-driving parameters.

Very early in small-crack research, the phenomenon of fatigue-crack closure [11] was recognized as a possible explanation for rapid small-crack growth rates (see for example Ref. 12). Fatigue crack closure is caused by residual plastic deformations left in the wake of an advancing crack. Only that portion of the load cycle for which the crack is fully open is used in computing an effective stress-intensity factor range (ΔK_{eff}) from LEFM solutions. A small crack initiating at an inclusion particle, a void or a weak grain does not have the prior plastic history to develop closure. Thus, a small crack may not be closed for as much of the loading cycle as a larger crack. If a small crack is fully open, the stress-intensity factor range is fully effective and the crack-growth rate will be greater than steady-state crack-growth rates. (A steady-state crack is one in which the

residual plastic deformations and crack closure along the crack surfaces are fully developed.) In contrast to small-crack growth behavior, the development of the large-crack threshold, as illustrated in Figure 1, has also been associated with an increase in crack-closure behavior as the load is reduced [13]. Thus, the steady-state crack-growth behavior may lie between the small-crack and large-crack threshold behavior, as illustrated by the dash-dot curve.

The purpose of this paper is to review the capabilities of a plasticity-induced crack-closure model [14,15] to correlate and to predict small- and large-crack growth behavior in several aluminum and titanium alloys under various load histories. Test results from the literature on aluminum alloys 2024-T3 [6,16,17], 7075-T6 [7,18], LC9cs [18] and 7475-T7351 [19,20] and on titanium alloys Ti-6Al-4V [21,22], IMI-685 [21-23] and Ti-17 [21,22] under constant-amplitude loading were analyzed with the closure model to establish an effective stress-intensity factor range against crack growth rate relation. For extreme or high crack-growth rates, equations to calculate a cyclic-plastic-zone corrected effective stress-intensity factor range are presented. These equations were developed from a cyclic J-integral and crack-closure analysis of large cracks [9] using the Dugdale model [24]. The effective stress-intensity factor range against crack growth rate relations were used in the closure model to predict large-crack growth under a single spike overload, an overload and underload, repeated spike overloads, Mini-TWIST [25] and Turbistan [26] loading. Using the closure model and some microstructural features, a total fatigue life prediction method is demonstrated on three aluminum alloys under various load histories. The load histories considered were the standardized FALSTAFF [27], Gaussian [28], TWIST [29] and Mini-TWIST [25] load spectra. The crack configurations used in these analyses are shown in Figure 2. They

were through crack configurations, such as center-crack and compact specimens (Fig. 2a), a corner crack in a bar (Fig. 2b) and surface or corner cracks at a notch or hole (Figs. 2c and 2d).

PLASTICITY-INDUCED CRACK-CLOSURE ANALYSIS

The analytical crack-closure model was developed for a central through crack in a finite-width specimen subjected to uniform applied stress [14,30]. The model was later extended to through cracks emanating from a circular hole and applied to the growth of small cracks [31]. The model was based on the Dugdale model [24], but modified to leave plastically deformed material in the wake of the crack. The details of the model and recent modifications to account for extremely high growth rates are discussed in Reference 32. The model was used to calculate crack-opening stresses as a function of crack length and load history. The applied stress level at which the crack surfaces are fully open is denoted as S_0' , the crack-opening stress. The crack-opening stresses calculated from the model for a through crack were also assumed to apply for surface or corner cracks at all locations along the crack front and the cracks were grown in both the a- and c-directions. Some special modifications are required where the crack front intersects a free surface [33]. The crack-opening stress is then used to calculate an effective stress-intensity factor range, ΔK_{eff} [11]. In turn, the crack-growth rate is calculated using a ΔK_{eff}-against-crack-growth-rate relation.

Effective Stress-Intensity Factor Range

Elber's effective stress-intensity factor range [11] was based on linear-elastic analyses. For high stress-intensity factors, such as those under high applied stresses, the plastic-zone sizes are no longer small compared to crack size, and linear-elastic analyses are inadequate. To

correct the analysis for plasticity, a portion of the Dugdale cyclic-plastic-zone length (ω) was added to the current crack length (c), like the well-known Irwin plastic-zone correction. Thus, the cyclic-plastic-zone corrected effective stress-intensity factor is

$$\Delta\bar{K}_{eff} = (S_{max} - S_o') \sqrt{\pi d}\ F_j(d/w, d/r, \ldots) \quad (1)$$

where S_{max} is the maximum applied stress, S_o' is the crack-opening stress, $d = c + \gamma\omega$, γ was determined to be 0.25 on the basis of a cyclic J-integral analysis [9], ω is the closure-corrected cyclic- plastic-zone size, and F_j is the usual boundary-correction factor evaluated at the fictitious crack length, d. The cyclic plastic-zone size is greatly influenced by closure because contact forces tend to support the crack surfaces and reduce the amount of reverse yielding. An estimate for the closure-corrected cyclic-plastic-zone size is

$$\omega = (\rho/4)\ (1 - R_{eff})^2 = (\rho/4)\ (1 - S_o'/S_{max})^2 \quad (2)$$

where ρ is the Dugdale plastic-zone size and is calculated using the maximum applied stress and $\alpha\sigma_o$. For other crack configurations, the plastic-zone size is estimated by using the small-scale yielding solution

$$\rho = \pi/8\ (K_{max}/\alpha\sigma_o)^2 \quad (3)$$

The flow stress σ_o is the average between yield stress and ultimate tensile strength. A constraint factor, α, was used to elevate the flow stress at the crack tip to account for three-dimensional stress states [14]. The bounds for the constraint factor are $\alpha = 1$ for plane-stress conditions and $\alpha = 3$ for plane-strain conditions. At present, the constraint factor is used as a fitting parameter to correlate crack-growth rate data under constant-amplitude loading for different stress ratios. However, tests conducted under single-spike overloads seem to be more sensitive to state-of-stress

effects and may be a more appropriate test to determine the constraint factor.

Constant-Amplitude Loading

In Reference 34, crack-opening stress equations for constant-amplitude loading were developed from the analytical crack-closure model (S_o) calculations for a center-crack tension specimen. These equations gave S_o as a function of stress ratio (R), maximum stress level (S_{max}/σ_o) and the constraint factor (α). To correct the previous crack-opening stress equations for extremely high crack-growth rates, a modification was developed in Reference 15 and is given by

$$S_o'/S_{max} = S_o/S_{max} + 0.3\ \sigma_o\ \sqrt{\Delta c/c}\ /(S_{max}F) \qquad (4)$$

where S_{max} is the maximum applied stress, Δc is the crack-growth increment (or rate per one cycle) and c is the current crack length. The boundary-correction factor, F, for the center-crack tension specimen was included to account for the influence of finite width. See Reference 32 for details on how Equation (4) is applied to compact specimens. The crack-opening stress equations for S_o will be presented later. Comparisons with the modified model showed that Equation (4) was reasonably accurate for a wide range in constant-amplitude loading conditions for S_{max}/σ_o less than about 0.6. The difference between S_o' and S_o was only significant (greater than a 2 percent effect on crack-opening stresses) for crack-growth rates greater than about 10^{-2} mm/cycle. For $S_{max}/\sigma_o > 0.6$, the crack-opening stresses should be calculated from the model instead of Equation (4).

The crack-opening stress equations for S_o will be presented here for completeness. These equations were developed by fitting to the calculated results from the model [34]. The equations are

$$S_o/S_{max} = A_0 + A_1R + A_2R^2 + A_3R^3 \quad \text{for } R \geq 0 \qquad (5)$$

and $S_o/S_{max} = A_0 + A_1 R$ for $R < 0$ (6)

where $S_{max}/\sigma_o < 0.8$ and $S_{min}/\sigma_o > -1$. If S_o/S_{max} is less than R, then $S_o/S_{max} = R$, and if S_o/S_{max} is negative, then $S_o/S_{max} = 0$. The A_i coefficients are functions of α and S_{max}/σ_o and are given by:

$$\left.\begin{aligned} A_0 &= (0.825 - 0.34\alpha + 0.05\alpha^2)\,[\cos(\pi S_{max} F/2\sigma_o)]^{1/\alpha} \\ A_1 &= (0.415 - 0.071\alpha)\, S_{max} F/\sigma_o \\ A_2 &= 1 - A_0 - A_1 - A_3 \\ A_3 &= 2A_0 + A_1 - 1 \end{aligned}\right\} \quad (7)$$

for $\alpha = 1$ to 3. Again, the boundary-correction factor, F, was added to these equations to account for the influence of finite width on crack-opening stresses. These equations are used to correlate fatigue crack-growth rate data to obtain effective stress-intensity factor range against crack-growth rate relations.

Equations (4) to (7) give approximate crack-opening stress equations that agree fairly well with results from the modified closure model. Some typical comparisons between the equations and the model for a crack in a titanium alloy are shown in Figures 3 and 4. To severely test the equations, variable constraint (α = 2.4 for rates less than 1E-04 mm/cycle and α = 1.2 for rates greater than 1E-03 mm/cycle) was used [35]. Figure 3 shows results for a crack in an infinite plate for low R; and Figure 4 shows results for a finite-width plate for low and high R. The dotted lines indicate the R ratio and the solid curves show results from the model. The crack-length-against-cycles results from the model were used to develop ΔK-rate data to be analyzed with the crack-opening stress equations, as if these data were from tests. The dashed curves show results from the equations. For constant α regions in Figures 3 and 4, the results from the equations agreed well with the model. Some differences were observed in the

transition region between α = 2.4 to 1.2 because the equations were originally developed for steady-state, constant-constraint conditions. In Figure 3, the maximum error in calculating ΔK_{eff} was 4 percent. For R = 0.1 case in Figure 4, the maximum error was about 10 percent in calculating ΔK_{eff} but this occurred as the crack was growing to failure. The small vertical lines indicate the corresponding life ratio (N/N_f), in addition to indicating regions of constant constraint.

Spectrum Loading

For variable-amplitude and spectrum loading, the crack-closure model must be used to compute the crack-opening stress history. Some typical crack-opening stresses under the Mini-TWIST load sequence for a small surface crack in a single-edge-notch-tension (SENT) specimen (Fig. 2c) and for a large crack in the center-crack- tension specimen will be presented in the following sections.

Small crack. In the small-crack simulation, an initial defect size of a_i = 3 μm and c_i = 9 μm was used. This size corresponds to inclusion-particle sizes that initiate cracks in some aluminum alloys [6,7]. Variable constraint was selected for this simulation. The constraint factor (α) was 1.8 for crack-growth rates less than 7E-04 mm/cycle and 1.2 for rates greater than 7E-03 mm/cycle. Figure 5 shows crack-opening stress (normalized by the maximum stress in the spectrum) plotted against the ratio of applied cycles to cycles-to-failure (N/N_f). The predicted cycles to failure, N_f, was about 800,000 cycles. These results show that the opening stresses start near the minimum stress in the spectrum and rise as the crack grows. Crack-opening stresses tended to level off for N/N_f between 0.7 and 0.9. The rapid jump in S_0'/S_{max} for an N/N_f ratio of about 0.92 was caused by the change in constraint from 1.8 to 1.2 at the higher crack-growth

rates. The surface crack became a through crack (a/t = 1) at an N/N_f ratio of about 0.9.

Large crack. Figure 6 shows some of the calculations from the model for a large crack under spectrum loading. The initial crack length was selected as 6 mm. Again, the crack-opening stresses have been normalized by S_{max}. From a life ratio (N/N_f) of about 0.05 to 0.65, the crack-opening stresses tended to oscillate about a mean value. The constraint factor during most of these calculations was 1.8. Beyond a life ratio of about 0.65, the constraint factor of 1.2 was activated and higher crack-opening stresses were calculated.

LARGE-CRACK GROWTH BEHAVIOR

To make life predictions, ΔK_{eff} (or $\Delta \bar{K}_{eff}$) as a function of the crack-growth rate must be obtained for the material of interest. Fatigue crack-growth rate data should be obtained over the widest possible range in rates (from threshold to fracture), especially if spectrum load predictions are required. Data obtained on the crack configuration of interest would be helpful but is not essential. The use of the plasticity-corrected stress-intensity factor is only necessary if severe loading (such as low cycle fatigue conditions) are of interest. Most damage-tolerant life calculations can be performed using the linear elastic stress-intensity factor analysis with crack-closure modifications. Herein, the elastic ΔK_{eff} analysis will be used unless otherwise stated.

Constant-Amplitude Loading

Under constant-amplitude loading, the only unknown in the analysis is the constraint factor, α. The constraint factor is determined by finding (by trial-and-error) an α value that will correlate the constant-amplitude fatigue-crack-growth-rate data over a wide range in stress ratios, as shown

in References 30 and 34. This correlation should produce a unique relationship between ΔK_{eff} (or $\Delta \bar{K}_{eff}$) and crack-growth rate.

In the large-crack-growth threshold regime for some materials, the plasticity-induced closure model may not be able to collapse the threshold (ΔK-rate) data onto a unique ΔK_{eff}-rate relation because of other forms of closure. Roughness- and oxide-induced closure (see Ref. 36) appear to be more relevant in the threshold regime than plasticity-induced closure. However, further study is needed to assess the interactions between plasticity-, roughness- and oxide-induced closure in this regime. If the plasticity-induced closure model is not able to give a unique ΔK_{eff}-rate relation in the threshold regime, then high stress ratio ($R \geq 0.7$) data may be used to establish the ΔK_{eff}-rate relation but ignoring the large-crack thresholds.

In the following, the ΔK_{eff}-rate relations for two aluminum alloys and one titanium alloy will be presented and discussed. Similar procedures were used to establish the relationships for all materials used in this study. The large-crack results for 7075-T6 aluminum alloy are shown in Figure 7 for data generated at two different laboratories and at three stress ratios [18]. The data collapsed into a narrow band with several transitions in slope occurring at about the same rate for all stress ratios. Some differences were observed in the threshold regime. For these calculations, a constraint factor (α) of 1.8 (nearly equivalent to Irwin's plane-strain condition) was used for rates less than 7E-04 mm/cycle (start of transition from flat-to-slant crack growth) and α equal to 1.2 was used for rates greater than 7E-03 mm/cycle (end of transition from flat-to-slant crack growth). For intermediate rates, α was varied linearly with the logarithm of crack-growth rate. The values of α were selected by trial-and-error.

The solid symbols (see upper left-hand portion of figure) denote measured rates at the end of transition from flat-to-slant crack growth [18,37]. It has been proposed in Reference 35 that the flat-to-slant crack-growth transition region may be used to indicate a change from nearly plane-strain to plane-stress behavior and, consequently, a change in constraint. In the low crack-growth rate regime, near and at threshold, some tests [13] and analyses [31] have indicated that the threshold develops because of a rise in the crack-opening-stress-to-maximum-stress ratio due to the load-shedding procedure. In the threshold regime then, the actual ΔK_{eff}-rate data would lie at lower values of ΔK_{eff} because the rise in crack-opening stress was not accounted for in the current analysis. For the present study, an estimate was made for this behavior and it is shown by the solid line below rates of about 2.0E-6 mm/cycle. The baseline relation shown by the solid line will be used later to predict large-crack growth under the Mini-TWIST load sequence.

Figure 8 shows the ΔK_{eff}-rate relation for large cracks in 7475-T7351 aluminum alloy. These data cover a very wide range in stress ratio [19] and the data correlated quite well with a constant constraint factor of 1.9. The 7475 material was thicker than the 7075 material shown in Figure 7. For thicker materials, the loss of constraint, as shown for the thin 7075, may occur at higher values of ΔK_{eff} than those shown for the thinner material. Consequently, a constant constraint factor was used over the whole rate range. Further analytical studies are needed, however, to establish constraint variations. A ΔK_{eff}-rate relation that extends down to much lower rates would be required for general application, but for the present purpose this correlation will be sufficient. The baseline relation (solid line) will be used later to predict crack-growth rates after a single spike overload and after a single spike overload followed by an underload.

The ΔK_{eff}-rate relations for IMI-685 titanium alloy compact and corner-crack specimens are shown in Figures 9 and 10, respectively. This material was selected to be analyzed because "roughness-induced" closure was expected to be prevalent. These data also illustrate two difficulties with correlating test data using the plasticity-induced closure model. First, the high R ratio results tend to deviate from the low R ratio results near the end of the tests. These specimens were cycled to failure and the last few data points were taken immediately before the specimen failed. Using a fracture toughness K_c = 80 MPa-$\sqrt{m}$, the high R ratio tests are predicted to fail at a ΔK_{eff} value of 23 MPa-$\sqrt{m}$. Thus, fitting the ΔK_{eff} relation to the low R ratio results (solid curve) will allow accurate life prediction at high rates for both the low and high R ratio conditions. The second difficulty with the model occurs in the threshold regime and shows that threshold data (load-reduction tests) begin to form bands of data as a function of R (see Fig. 9). The steady-state crack-opening stress equations do not account for any load-reduction effects nor roughness-induced closure which is expected to be dominate in the IMI-685 alloy. Because cracks in the high R ratio tests are expected to be fully open, these results were used to determine the ΔK_{eff} relation at the low rates. The low crack-growth rate data on the corner-crack specimens (Fig. 10) were generated with initial crack sizes of about 250 μm in length. Here the low and high R ratio data do not show any significant separation using the steady-state crack-opening stress equations. The baseline curves for compact and corner-crack specimens will be used later to make life predictions under repeated spike overloads and Turbistan.

Spike Overload and Underload

For variable-amplitude or spectrum load crack-growth predictions, the constraint factor (α) should also be verified by some simple tests, such as

crack growth after a single-spike overload. Constraint factors appear to be more sensitive to crack-growth delays caused by single-spike overloads than to crack growth under constant-amplitude loading at different stress ratios. Higher values of constraint (α) will cause less load-interaction effects, such as retardation or acceleration, than lower values of constraint. Thus, spike-overload tests may be more useful in establishing values of α than constant-amplitude tests.

A comparison of measured and predicted rates for large cracks after a single spike overload and after a single spike overload followed by an underload are shown in Figure 11. Cracks were grown under constant-amplitude loading (R = 0.4 with K_{max} = 19.7 MPa-$\sqrt{m}$) to a crack length of 12 mm. In one case, a single overload, K_{OL} = 31.4 MPa-$\sqrt{m}$, was applied and then the test was returned to constant-amplitude loading. The second case was identical to the first case, except that an underload K_{UL} = -3.9 MPa-$\sqrt{m}$ was applied immediately after the overload. Two methods were used to measure crack length and rates in the 7475 alloy [20]: the direct-current potential method (solid symbols) and the scanning-electron microscope (open symbols). The predicted results using the closure model with α = 1.9 (curves) agreed well with the test results, especially for the overload-underload case. For the overload case, the experimental rates did not appear to stabilize at the pre-overload rates as quickly as the predictions. These results indicate that the constraint factor of 1.9 is appropriate for these conditions. But overloads at higher K_{OL} values would be expected to cause some loss of constraint (lower α). Under these conditions, the analyses using an α = 1.9 would be expected to predict higher rates and less retardation than the tests. Thus, variable constraint may be needed to predict the behavior.

Repeated Spike Overloads

Figure 12 shows a comparison of measured and predicted ΔK-rate results for repeated spike overloads applied to compact and corner-crack specimens made of the IMI-685 titanium alloy. These tests were conducted under constant-amplitude loading (R = 0.1) with an overload (P_{OL} = 1.7 P_{max}) applied every 1,000 cycles [21]. In view of the large scatter in the test data, the overall trends in the predicted results for the corner-crack configuration agreed well with the test results at low rates. However, the predicted rates tended to be somewhat high in the middle and upper ranges. Although the overall predicted results for the compact specimen agreed fairly well with the test data, the test results on each individual specimen were not modelled very accurately. The measured rates on one of the compact specimens in the beginning of the test were much lower than predicted. The oscillating behavior in the predicted results at high rates was caused by averaging rates over less than 1000 cycles, thus accelerations and retardations during and after the spike overload are being shown.

Table 1 shows a comparison of predicted-to-test lives (N_p/N_t) for all three titanium alloys and the two crack configurations analyzed. The predicted results on the repeated-spike overloads were generally within about 20 percent of the test results. These results are presented and discussed in Reference 22.

Spectrum Loading

In Reference 18, several tests were conducted on center-crack tension specimens to monitor large-crack growth in 7075-T6 aluminum alloy under the Mini-TWIST load spectrum. Five tests were conducted at three different mean-flight stress (S_{mf}) levels. These test results (symbols) are shown in Figure 13. Variable constraint (α varied from 1.8 at low rates to 1.2 at high rates) was used to predict spectrum crack growth. The predicted

results were within ± 25 percent of the test results. To illustrate the importance of variable constraint for spectrum crack growth in thin-sheet aluminum alloys, a second set of predictions (not shown) were made using a "constant" constraint factor of 1.8. The predicted results for the two lowest mean-flight stress levels were similar to those shown in Figure 13. However, the prediction of cycles to failure for the highest mean-flight stress level case was considerably lower (about a factor of three) than the test results.

A comparison of measured [22] and predicted lives for cracks in compact and corner-crack specimens made of the three titanium alloys and subjected to the Turbistan [26] load sequence are also shown in Table 1. The predicted results under the Turbistan loading were generally within a factor of two of the test data, but most of the results were within about ± 25 percent. In fatigue-crack growth life prediction methodology, any analysis methods that predict within a factor-of-two of test data are considered satisfactory. The approach presented here, generally, did much better.

SMALL-CRACK GROWTH BEHAVIOR

In the following, comparisons are made between measured and predicted crack-shape changes and crack-growth rates for small surface cracks at the edge of a notch (Fig. 2c) in 2024-T3 aluminum alloy [6]. Figures 14 shows the crack-depth-to-crack-length (a/c) ratio plotted against the crack-depth-to-sheet-half-thickness (a/t) ratio. The solid symbols show the sizes and shapes of inclusion-particle clusters or voids which initiated small cracks. Measured a/c and a/t ratios (open symbols) were determined from an experimental method where specimens were broken early in life. In the analysis, three different initial crack shapes and sizes were used. In one case, the initial crack was an average of the inclusion-particle sizes, whereas the other two crack sizes and shapes were arbitrarily selected. The

curves show the calculations using stress-intensity factor equations [9] and a ΔK_{eff}-rate (dc/dN) relation established from large-crack data [35]. The crack-growth rate relation for da/dN was assumed to be the same as dc/dN. Although a large amount of scatter was evident, all predictions tended to follow the general trend in the test data for a/t ratios greater than 0.05. These analyses also show that small cracks tend to approach very rapidly a preferred crack shape of about an a/c ratio of 1.1 for a large part of their growth through the thickness. For deep cracks (large a/t), the cracks begin to grow more rapidly along the bore of the notch than in the length direction, causing a/c to increase rapidly.

At this point, the small-crack data generated in the AGARD Cooperative Test Program [6] on 2024-T3 aluminum alloy will be analyzed using the plasticity and closure model analyses previously presented to assess the influence of plasticity on crack-growth rates. The results from these analyses are presented in terms of ΔK plotted against crack-growth rate as shown in Figure 15. The dash-dot curve shows the ΔK-rate data generated on large cracks; and the dotted curve is the effective stress-intensity factor curve. The effective curve was based on elastic stress-intensity factors and crack-closure analysis with $\alpha = 1.73$. Because small cracks were assumed to have no plastic wake on the first cycle, the elastic analysis (dashed curve) starts on the ΔK_{eff} curve and approaches the large-crack curve as the plastic wake develops. As shown by the difference between the solid and dashed curves, the plasticity effects are negligibly small and the crack-closure transient is shown to be the dominant small-crack effect. See Reference 9 for more details and analyses of other small-crack data.

FATIGUE-LIFE PREDICTION METHODOLOGY

The small-crack analyses using elastic or elastic-plastic effective stress-intensity factor ranges will be used in the following sections to

predict the fatigue (S-N) behavior for notched specimens made of three aluminum alloys and tested under either constant-amplitude or various spectrum loadings. In general, the elastic ΔK_{eff} analyses will be used unless otherwise stated.

Constant-Amplitude Loading

Landers and Hardrath [16] conducted fatigue tests on 2024-T3 aluminum alloy sheet material with specimens containing a central hole. These results are shown in Figure 16 as symbols. The solid and dashed curves show predictions using large-crack growth rate data (ignoring the large-crack threshold) and an initial crack size based on an average inclusion-particle size [6]. The large-crack growth rate properties are given in Reference 35 for elastic stress-intensity factor analysis (see dotted curve in Fig. 15). The crack-growth rate properties using the elastic-plastic effective stress-intensity factor analysis (Eqn. (1)) were obtained from a reanalysis of the large-crack data. Both predictions agreed near the fatigue limit but differed substantially as the applied stress approached the flow stress (σ_0 = 425 MPa). In these predictions, a ΔK-effective threshold for small cracks was 1.05 MPa-$\sqrt{m}$ (see Ref. 35). The predicted fatigue limit agreed well with experimental data for tests up to 10^7 cycles. However, test failures were still occurring beyond 10^7 cycles. This may indicate that fatigue damage or small-crack growth is continuing below the lower test levels. This would indicate that the lower portion of the effective stress-intensity factor curve, as shown in Figure 15, should have a steep slope instead of being vertical. Above a stress level of about 250 MPa, the results from the elastic and elastic-plastic analyses differ substantially. The results from the elastic-plastic analyses agreed well with the test data and substantiates the cyclic-plastic-zone corrected stress-intensity factor. Static tests (tensile strength) on this configuration gave an average

failure stress of about 400 MPa for three tests. The highest applied stress predicted from the elastic-plastic analysis for one cycle was 422 MPa (plastic-zone extended across the net section).

Spectrum Loading

Comparisons of experimental and predicted fatigue lives of notched 2024-T3 aluminum alloy sheet specimens under FALSTAFF, Gaussian and TWIST load sequences are shown in Figure 17. These tests were conducted on SENT specimens [6,17] that were cycled until a crack had grown across the full sheet thickness, referred to as breakthrough. The predictions were made using the same initial crack size as that used for the previous constant-amplitude predictions. Elastic and elastic-plastic ΔK_{eff}-rate relations and the closure model were used. The predicted lives agreed well with the test data and showed that plasticity effects were small.

Experimental and predicted results for fatigue tests conducted on bare 7075-T6 and clad LC9cs alloy specimens under the Mini-TWIST spectrum are shown in Figure 18. These tests were conducted on SENT specimens [18] but they were cycled to failure. The solid and dashed curves show predictions for each alloy using elastic ΔK_{eff}-rate relations and the initial defect sizes shown. The defect size for 7075-T6 was close to the average inclusion-particle size that initiated cracks, whereas the initial crack size for the clad alloy LC9cs was somewhat larger than the cladding-layer thickness (50 to 70 μm). The predicted lives were in reasonable agreement with the test results (symbols) but the predicted lives tended to fall on the lower bound of the test data.

CONCLUDING REMARKS

The "plasticity-induced" crack-closure model was used to correlate large-crack data on several aluminum and titanium alloys under constant-

amplitude loading. A constraint factor, which accounts for three-dimensional state-of-stress effects, was used in determining the effective stress-intensity factor range against rate relations. These relations were then used to predict large-crack growth under variable-amplitude and spectrum loading (within ± 25 percent).

For small-crack growth at high stress levels, a cyclic-plastic-zone corrected effective stress-intensity factor range was presented and was applied to small-crack growth and fatigue-life predictions. A comparison of measured and predicted small-crack growth rates in an aluminum alloy showed that plasticity effects were negligibly small near the fatigue limit, and that the crack-closure transient was the dominant small-crack effect.

Using the crack-closure model and some microstructural features, such as inclusion-particle sizes and cladding-layer thickness, a total fatigue-life prediction methodology was demonstrated. Fatigue life of notched specimens made of three aluminum alloys were compared with predicted lives under either constant-amplitude or spectrum loading. The predicted results were well within a factor of two of the test data.

Further study is needed to analytically determine constraint variations along fatigue crack fronts in various materials and thicknesses. These constraint variations are needed to improve life predictions under aircraft spectrum loading, especially for thin-sheet materials. At low rates, the development of the large-crack threshold and its significance for design life calculations also needs further study.

REFERENCES

1. Gallagher, J. P.; Giessler, F. J.; Berens, A. P. and Engle, R. M., Jr., "USAF Damage Tolerant Design Handbook: Guidelines for the Analysis and Design of Damage Tolerant Aircraft Structures," AFWAL-TR-82-3073, May 1984.

2. Manning, S. D. and Yang, J. N., "USAF Durability Design Handbook: Guidelines for the Analysis and Design Aircraft Structures," AFWAL TR-83-3027, January 1984.

3. Small Fatigue Cracks, R. O. Ritchie and J. Lankford, eds., The Metallurgical Society, Inc., Warrendale, PA, 1986.

4. The Behaviour of Short Fatigue Cracks, K. J. Miller and E. R. de los Rios, eds., European Group on Fracture, Publication No. 1, 1986.

5. Rao, K. T. V. and Ritchie, R. O., Fatigue of Aluminum-Lithium Alloys, Lawrence Berkeley Laboratory, LBL-30176, January 1991.

6. Newman, J. C. Jr. and Edwards, P. R., Short-Crack Growth Behaviour in an Aluminum Alloy - an AGARD Cooperative Test Programme, AGARD R-732, 1988.

7. Short-Crack Growth Behavior in Various Aircraft Materials, P. R. Edwards and J. C. Newman, Jr., eds., AGARD Report No. 767, 1990.

8. El Haddad, M. H.; Dowling, N. E.; Topper, T. H. and Smith, K. N., J Integral Application for Short Fatigue Cracks at Notches, International Journal of Fracture, Vol. 16, No. 1, 1980, pp. 15-30.

9. Newman, J. C., Jr., Fracture Mechanics Parameters for Small Fatigue Cracks, Small Crack Test Methods, ASTM STP 1149, J. Allison and J. Larsen, eds., 1992, pp. 6-28.

10. Leis, B. N.; Kanninen, M. F.; Hopper, A. T.; Ahmad, J. and Broek, D., Critical Review of the Short Crack Problem in Fatigue, Engineering Fracture Mechanics, Vol. 23, 1986, pp. 883-898.

11. Elber, W., The Significance of Fatigue Crack Closure, Damage Tolerance in Aircraft Structures, ASTM STP 486, 1971, pp. 230-242.

12. Nisitani, H. and Takao, K. I., Significance of Initiation, Propagation and Closure of Microcracks in High Cycle Fatigue of Ductile Materials, Engineering Fracture Mechanics, Vol. 15, No. 3-4, 1981, pp. 445-456.

13. Minakawa, K. and McEvily, A. J., On Near-Threshold Fatigue Crack Growth in Steels and Aluminum Alloys, Proceedings of the International Conference on Fatigue Thresholds, Vol. 2, 1981, pp. 373-390.

14. Newman, J. C., Jr., A Crack-Closure Model for Predicting Fatigue Crack Growth under Aircraft Spectrum Loading, Methods and Models for Predicting Fatigue Crack Growth under Random Loading, J. B. Chang and C. M. Hudson, eds., ASTM STP 748, 1981, pp. 53-84.

15. Newman, J. C., Jr., Poe, C. C., Jr. and Dawicke, D. S., Proof Test and Fatigue Crack Growth Modeling on 2024-T3 Aluminum Alloy, Fourth International Conference on Fatigue and Fatigue Thresholds, 1990, pp. 2407-2416.

16. Landers, C. B. and Hardrath, H. F., Results of Axial-Load Fatigue Tests on Electropolished 2024-T3 and 7075-T6 Aluminum Alloy Sheet Specimens with Central Holes, NACA TN-3631, Mar. 1956.

17. Blom, A. F., Short Crack Growth under Realistic Flight Loading: Model Predictions and Experimental Results for AL 2024 and AL-LI 2090, Short-Crack Growth Behavior in Various Aircraft Materials, P. R. Edwards and J. C. Newman, Jr., eds., AGARD Report No. 767, 1990, pp. 6.1-6.15.

18. Newman, J. C., Jr.; Wu, X. R.; Swain, M. H.; Zhao, W.; Phillips, E. P. and Ding, C. F., Small-Crack Growth Behavior in High-Strength Aluminum Alloys - A NASA/CAE Cooperative Program, 18th Congress International Council of the Aeronautical Sciences, Sept. 20-25, 1992, ICAS-92-5.4.3.

19. Zhang, S.; Marissen, R.; Schulte, K.; Trautmann, K. -H.; Nowak, H. and Schijve, J., Crack Propagation Studies on Al 7475 on the Basis of Constant Amplitude and Selective Variable Amplitude Loading Histories, Fatigue and Fracture of Engineering Materials and Structures, Vol. 10, 1987, pp. 315-332.

20. Zhang, S.; Doker, H.; Nowak, H.; Schulte, K. and Trautmann, K. H., Improvements of Crack Propagation Analysis by More Exact Determination of K_{op}-Levels, Second Symposium on Fatigue Lifetime Predictive Techniques, ASTM, Pittsburgh, PA., 1992.

21. Raizenne, M. D., AGARD SMP Sub-Committee 33 Engine Disc Test Programme Fatigue Crack Growth Rate Data and Modeling Cases for Ti-6Al-4V, IMI-685 and Ti-17, LTR-ST-1785, National Research Council Canada, Nov. 1990.

22. AGARD Engine Disc Cooperative Test Programme, Jany, E. and Raizenne, M. D., eds., AGARD Report in progress, 1992.

23. Hicks, M. A.; Jeal, R. H. and Beevers, C. J., Slow Fatigue Crack Growth and Threshold Behaviour in IMI 685, Fatigue and Fracture of Engineering Materials and Structures, Vol. 6, No. 1, 1983, pp. 51-65.

24. Dugdale, D. S., Yielding of Steel Sheets Containing Slits, Journal of Mechanics and Physics of Solids, Vol. 8, Vol. 2, 1960, pp. 100-104.

25. Lowak, H.; deJonge, J. B.; Franz, J. and Schutz, D., Mini-TWIST--A Shortened Version of TWIST, LBF Report No. TB-146, Laboratorium fur Betriebsfestigkeit, 1979.

26. ten Have, A. A., Cold Turbistan - Final Definition of a Standardized Fatigue Test Loading Sequence for Tactical Aircraft Cold Section Engine Disc, NLR TR 87054 L, Nationaal Lucht-en Ruimtevaartlaborium, 1987.

27. van Dijk, G. M. and deJonge, J. B., Introduction to a Fighter Loading Standard for Fatigue Evaluation--FALSTAFF, NLR MP 75017 U, Nationaal Lucht-en Ruimtevaartlaborium, May 1975.

28. Huck, M.; Schutz, W.; Fischer, R. and Kobler, H. G., A Standard Random Load Sequence of Gaussian Type Recommended for General Application in Fatigue Testing, IABG Report No. TF-570 or LBF Report No. 2909, 1976.

29. deJonge, J. B.; Schutz, D.; Lowak, H. and Schijve, J., A Standardized Load Sequence for Flight Simulation Tests on Transport Aircraft Wing Structures (TWIST), NLR TR-73029 U, Nationaal Lucht-en Ruimtevaartlaborium, 1973.

30. Newman, J. C., Jr., Prediction of Fatigue-Crack Growth under Variable-Amplitude and Spectrum Loading using a Closure Model, Design of Fatigue and Fracture Resistant Structures, P. R. Abelkis and C. M. Hudson, eds., ASTM STP 761, 1982, pp. 255-277.

31. Newman, J. C., Jr., A Nonlinear Fracture Mechanics Approach to the Growth of Small Cracks, Behaviour of Short Cracks in Airframe Components, AGARD CP-328, 1983, pp. 6.1-6.26.

32. Newman, J. C., Jr., FASTRAN II - A Fatigue Crack Growth Structural Analysis Program, NASA TM 104159, February 1992.

33. Newman, J. C., Jr. and Raju, I. S., Prediction of Fatigue Crack-Growth Patterns and Lives in Three-Dimensional Cracked Bodies, Advances in Fracture Research, S. R. Valluri et.al., eds., 1984, pp. 1597-1608.

34. Newman, J. C., Jr., A Crack Opening Stress Equation for Fatigue Crack Growth, International Journal of Fracture, Vol. 24, 1984, R131-R135.

35. Newman, J. C.; Swain, M. H. and Phillips, E. P., An Assessment of the Small-Crack Effect for 2024-T3, Small Fatigue Cracks, Ritchie, R.O. and Lankford, J., eds., 1986, pp.427-452.

36. Ritchie, R. O. and Yu, W., Short Crack Effects in Fatigue: A Consequence of Crack Tip Shielding, Small Fatigue Cracks, R. O. Ritchie and J. Lankford, eds., 1986, pp. 167-189.

37. Vogelesang, L. B., The Effect of Environment on the Transition from Tensile Mode to Shear Mode during Fatigue Crack Growth in Aluminum Alloys, Delft Report LR-286, Delft University of Technology, 1979.

38. Newman, J. C., Jr.; Phillips, E. P.; Swain, M. H. and Everett, R. A., Jr., Fatigue Mechanics: An Assessment of a Unified Approach to Life Prediction, Advances in Fatigue Lifetime Predictive Techniques, M. R. Mitchell and R. W. Landgraf, ASTM STP 1122, 1992, pp. 5-27.

Table 1.- Ratio of Predicted to Experimental Crack Propagation Life for Three Titanium Alloys.

Material	Specimen	Load Sequence	
		Repeated Spike N_p/N_t	Turbistan N_p/N_t
Ti-6Al-4V (α = 1.9)	CT (a)	0.87	0.76
	CC (b)	0.87	2.12 (c)
IMI-685 (α = 1.8)	CT	0.95	1.13
	CC	0.78	0.57 (d)
Ti-17 (α = 2.0)	CT	0.99	0.89
	CC	0.86	0.95

(a) Compact tension specimen.
(b) Corner-crack tension specimen.
(c) Best prediction of five participants (N_p/N_t = 2.12 to 3.22).
(d) Lowest prediction of five participants (N_p/N_t = 0.57 to 1.95).

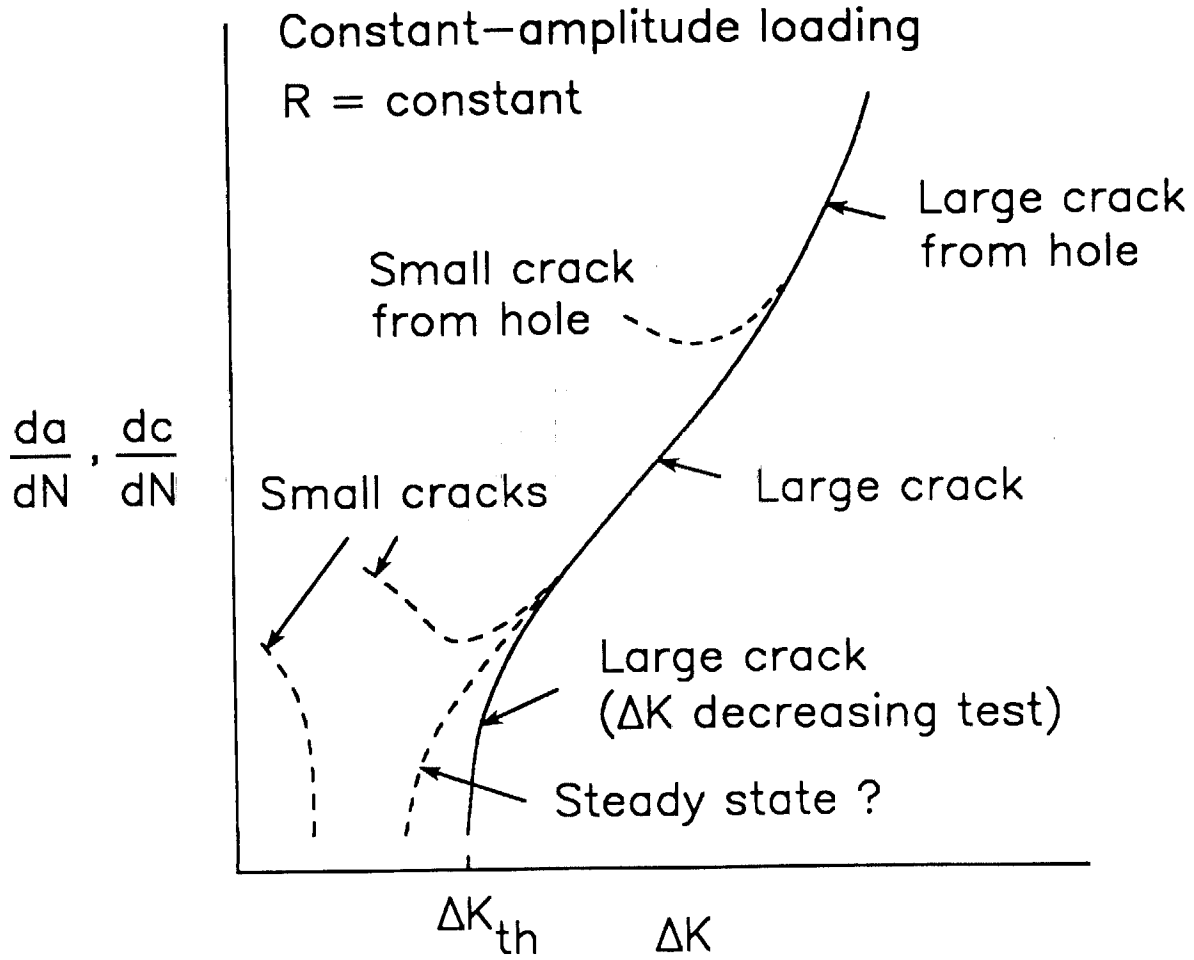

Figure 1.- Typical fatigue-crack-growth rate data for small and large cracks.

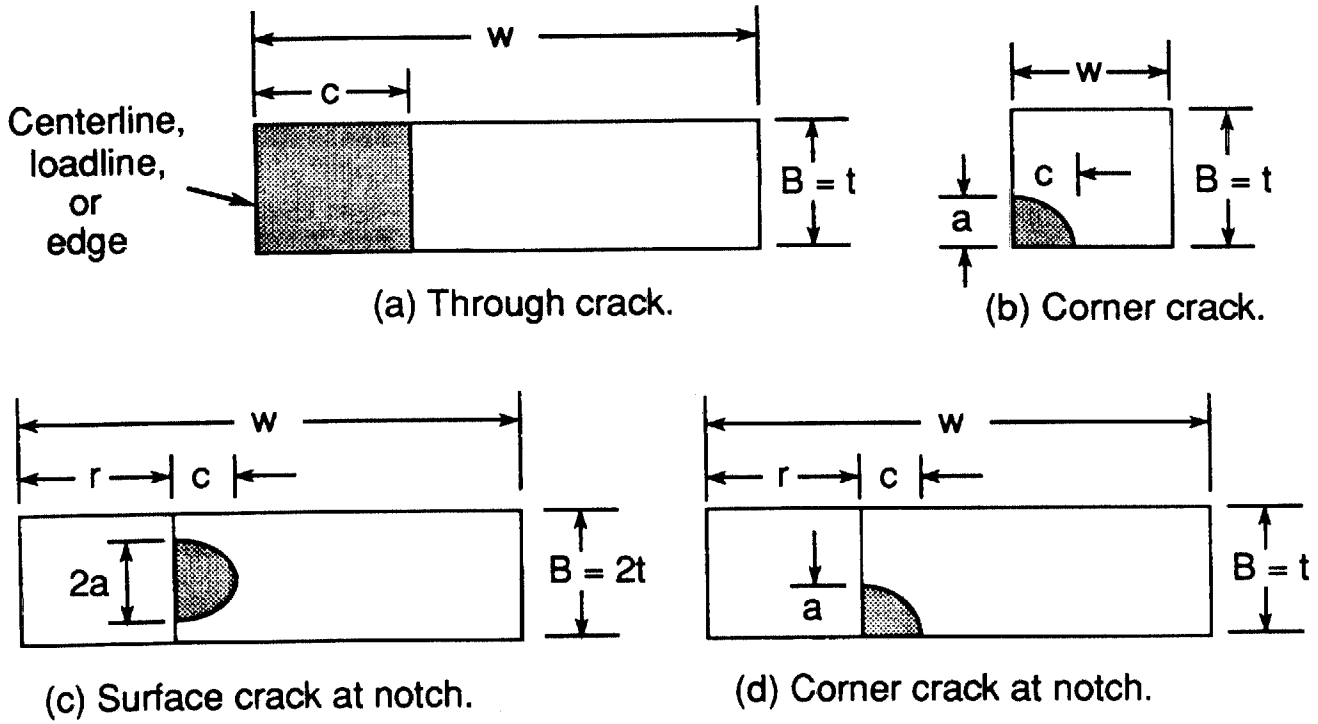

Figure 2.- Crack specimen configurations tested and analyzed.

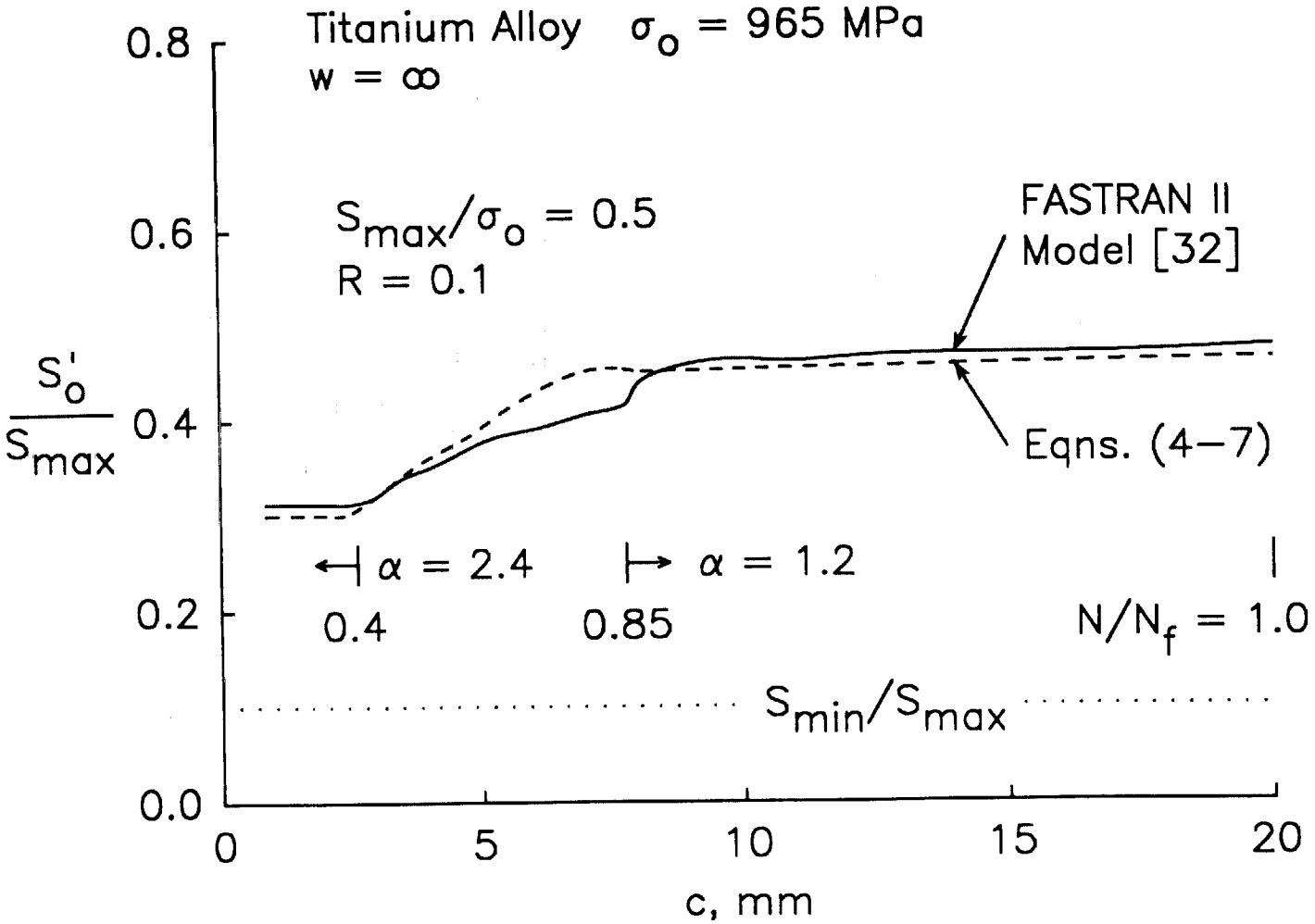

Figure 3.- Calculated crack-opening stresses for a large crack in an infinite plate made of a titanium alloy.

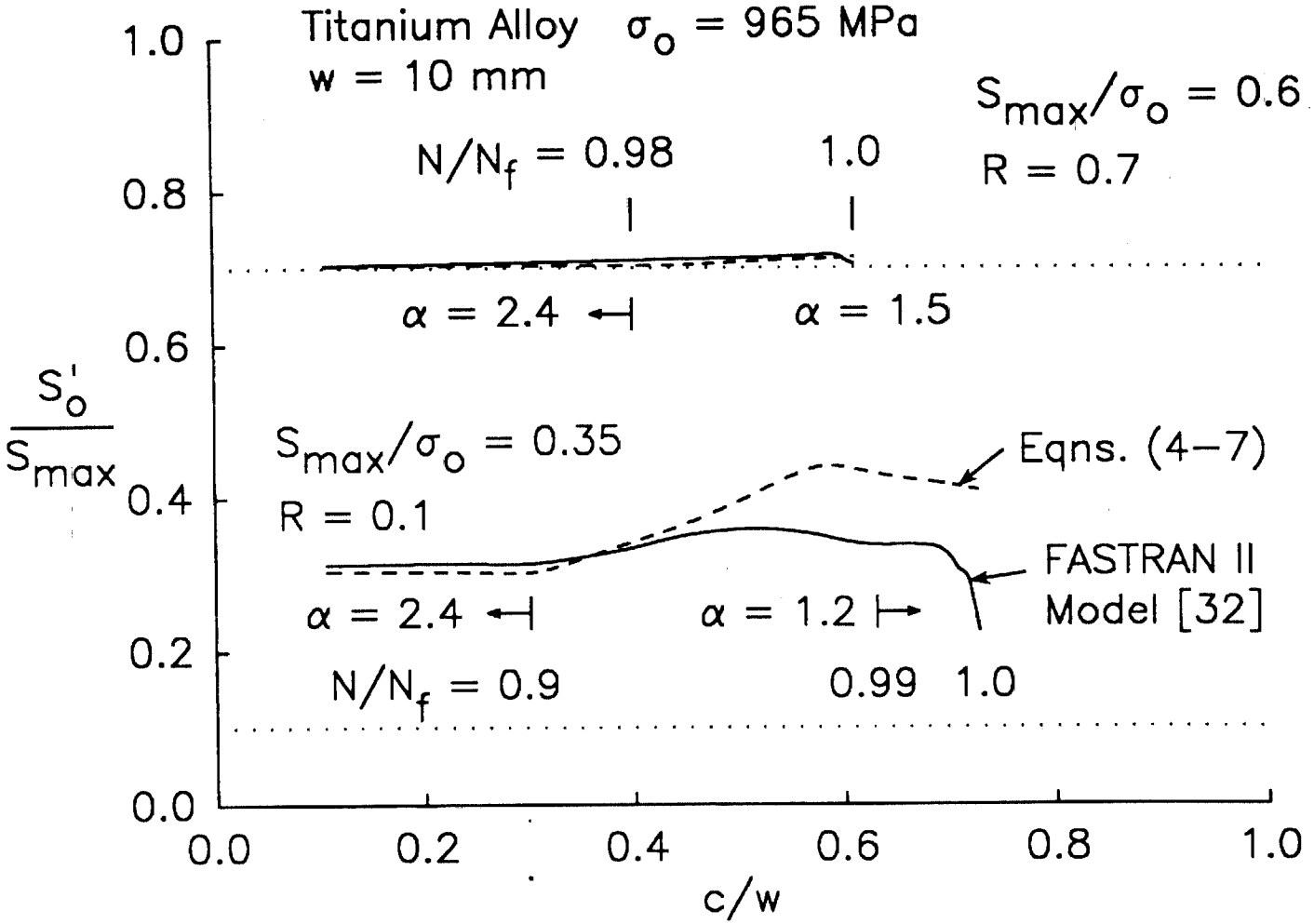

Figure 4.- Calculated crack-opening stresses for a large central crack in a finite-width specimen made of a titanium alloy.

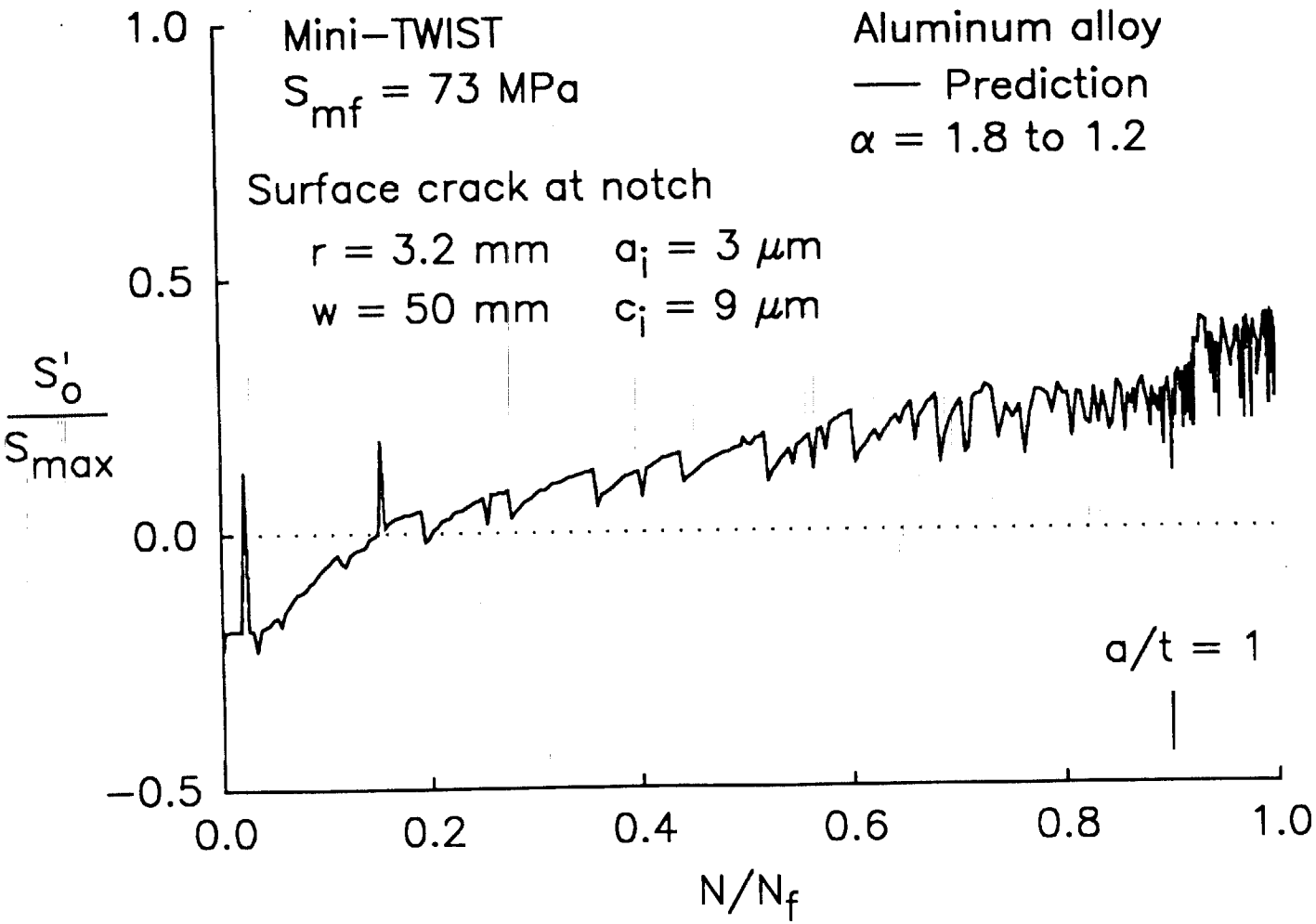

Figure 5.- Calculated crack-opening stresses for a small crack in an aluminum alloy under Mini-TWIST spectrum loading.

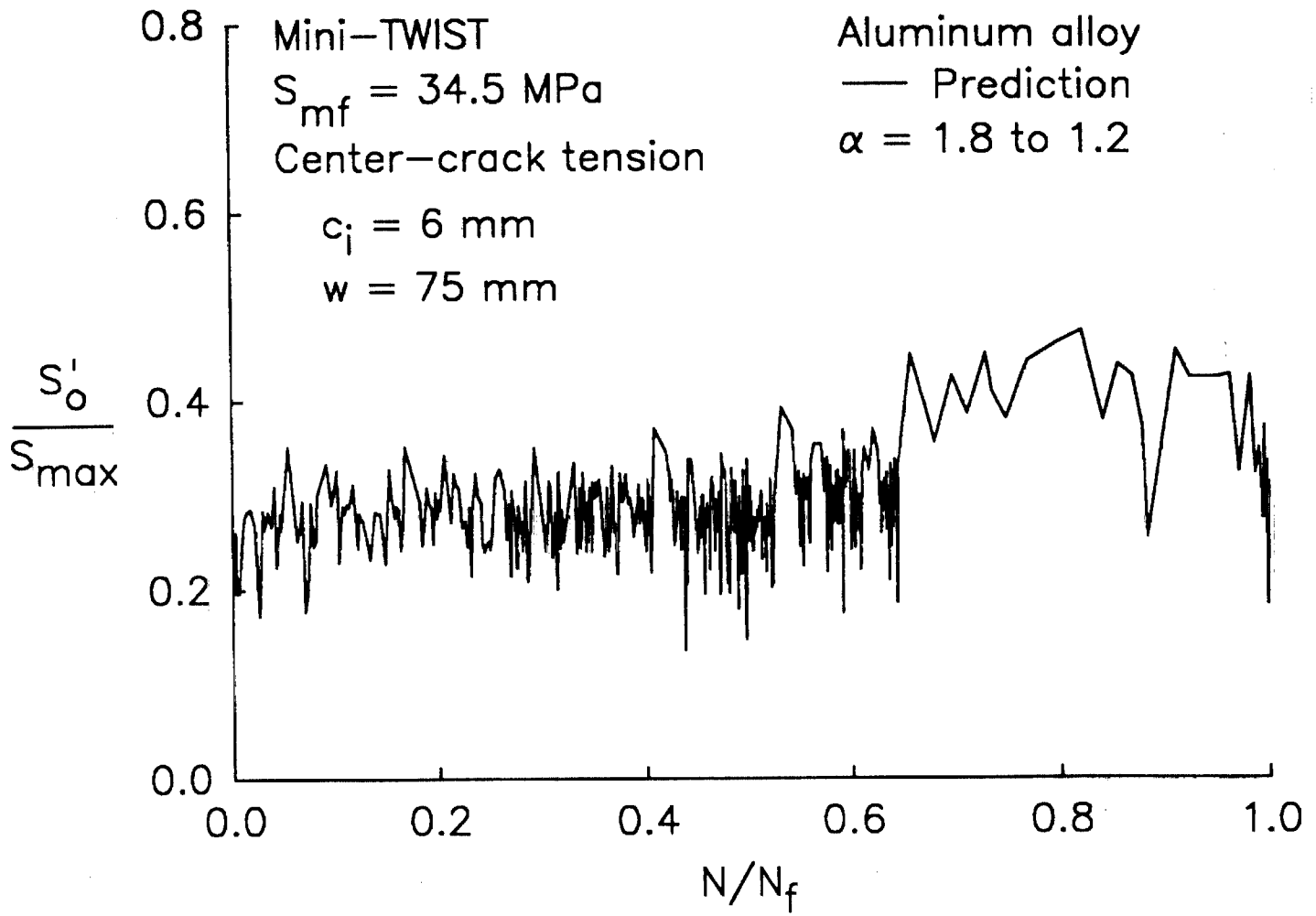

Figure 6.- Calculated crack-opening stresses for a large crack in an aluminum alloy under Mini-TWIST spectrum loading.

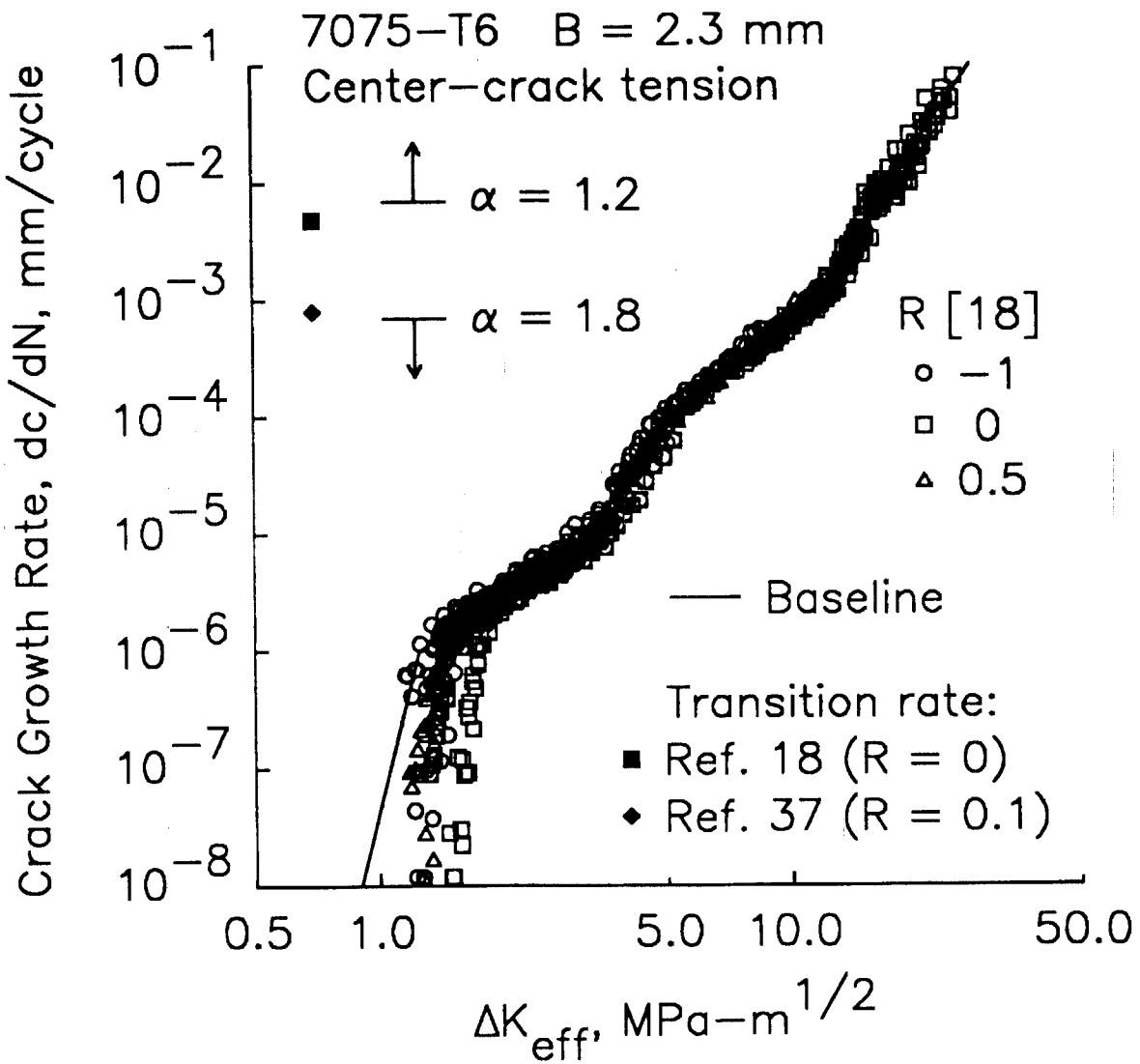

Figure 7.- Effective stress-intensity factor range against crack-growth rate for large cracks in 7075-T6 aluminum alloy.

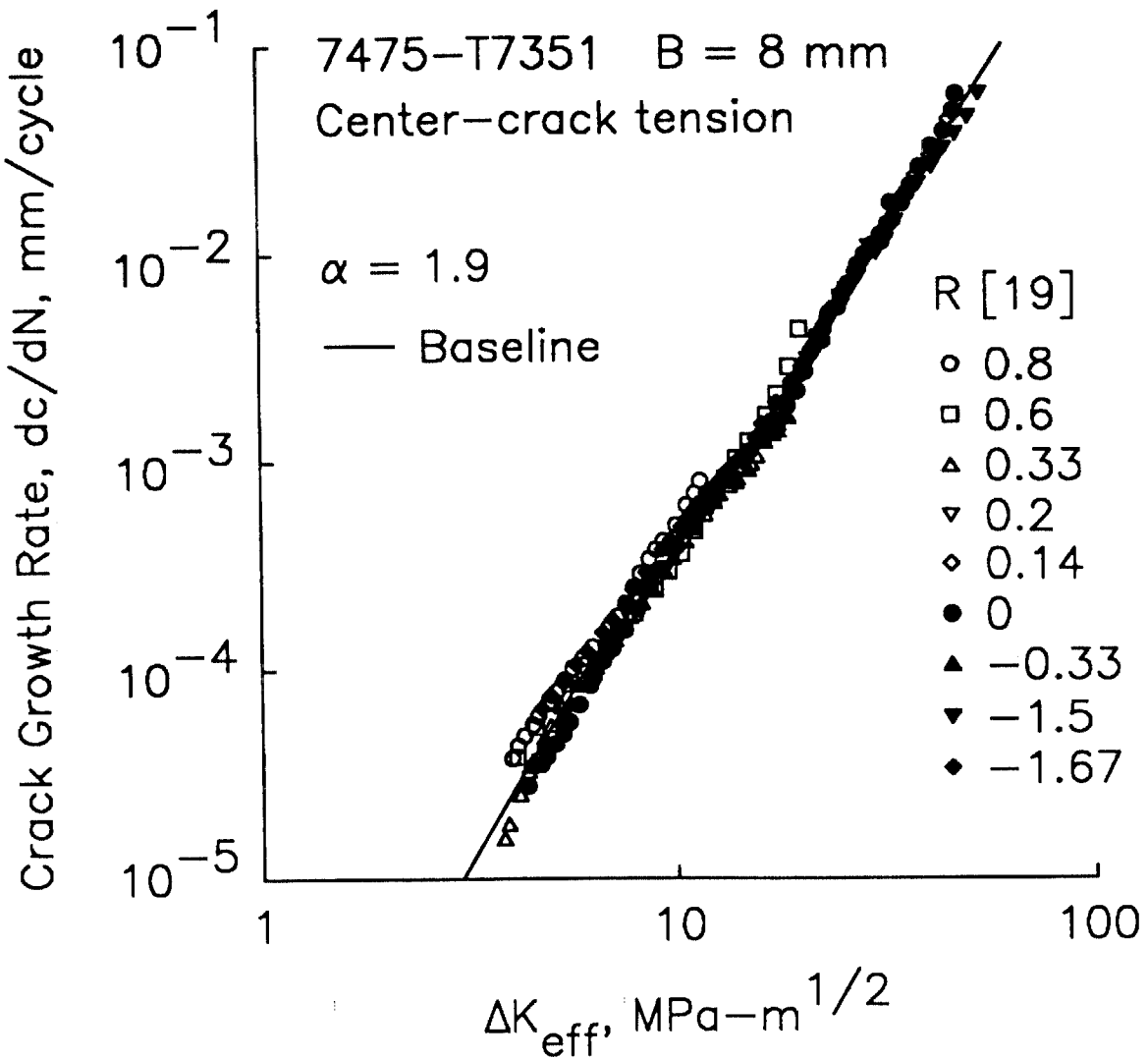

Figure 8.- Effective stress-intensity factor range against crack-growth rate for large cracks in 7475-T7351 aluminum alloy.

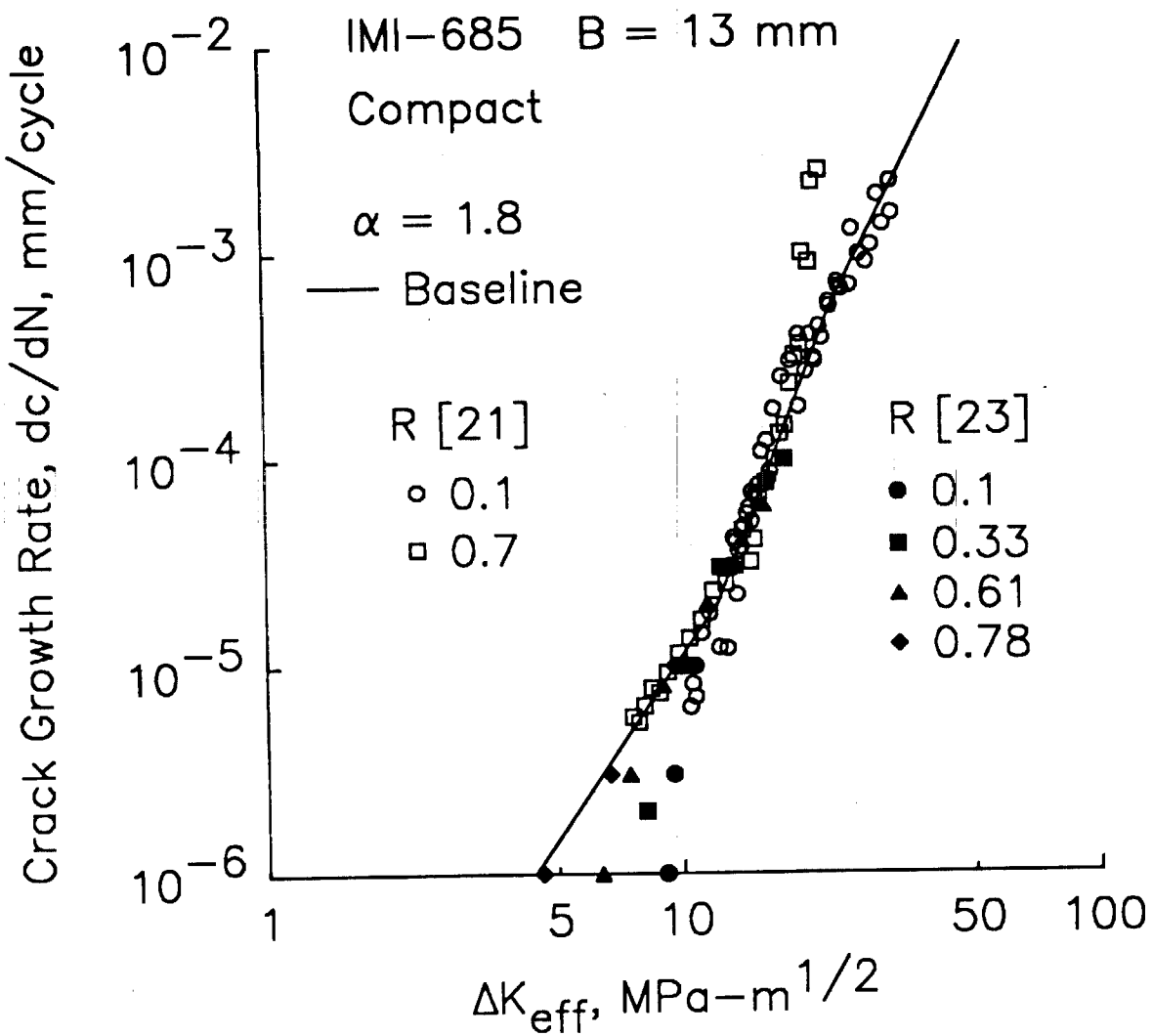

Figure 9.- Effective stress-intensity factor range against growth rate for large cracks in IMI-685 titanium alloy compact specimens.

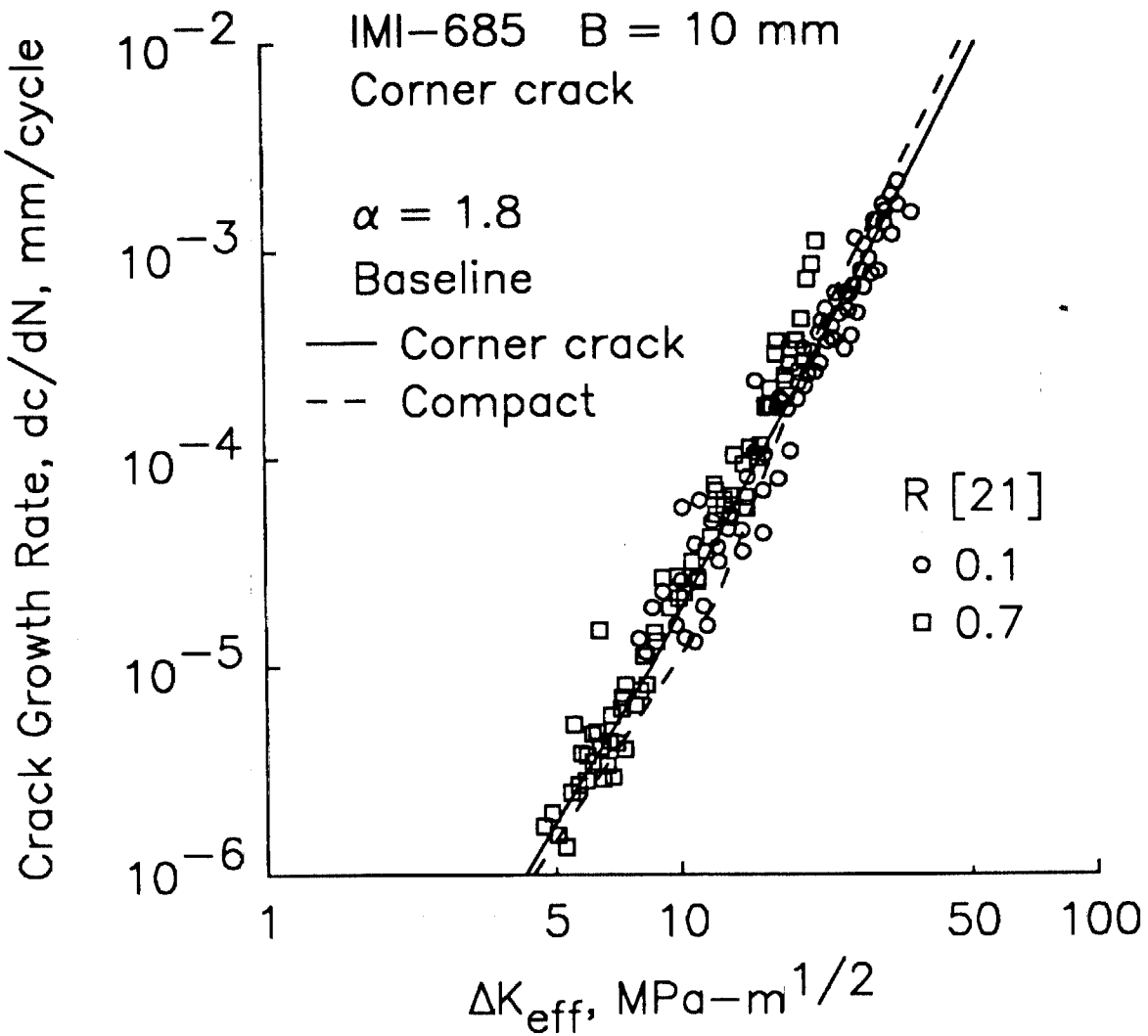

Figure 10.- Effective stress-intensity factor range against growth rate for cracks in IMI-685 titanium alloy corner-crack specimens.

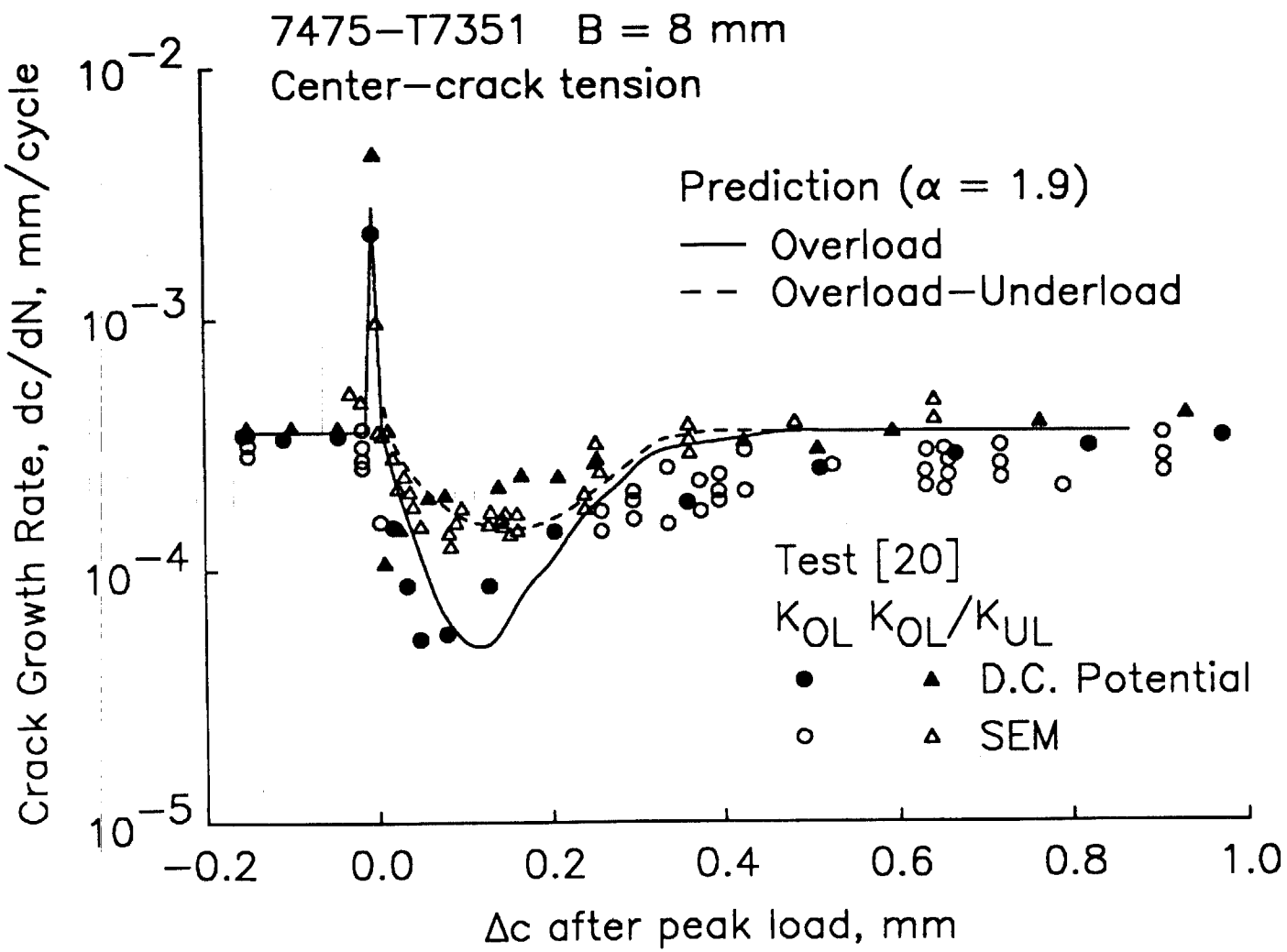

Figure 11.- Comparison of measured and predicted rates for large cracks after an overload and after an overload-underload sequence.

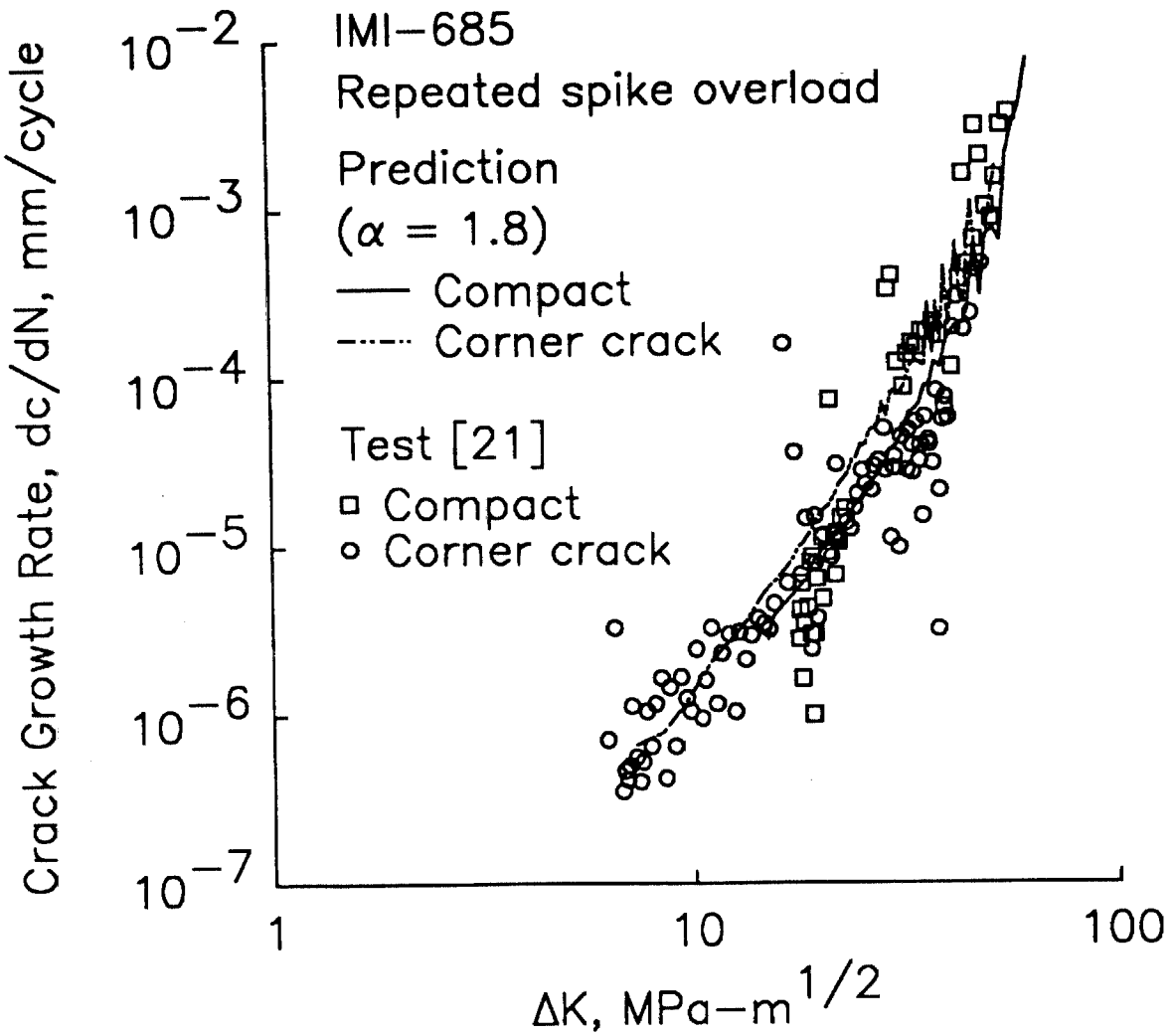

Figure 12.- Comparison of measured and predicted rates for large cracks under a repeated spike overload sequence.

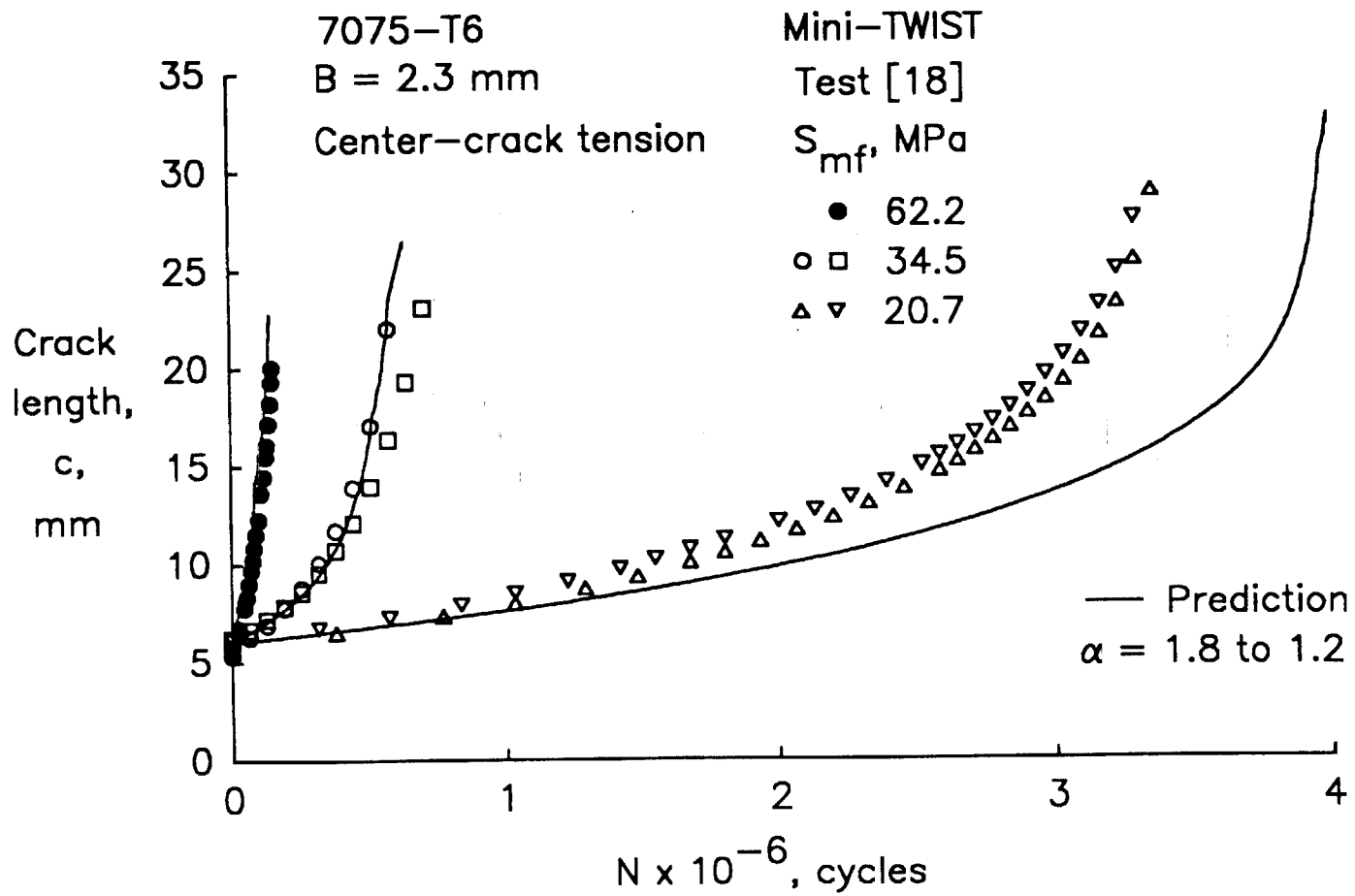

Figure 13.- Comparison of measured and predicted crack-length-against-cycles for large cracks under Mini-TWIST spectrum loading.

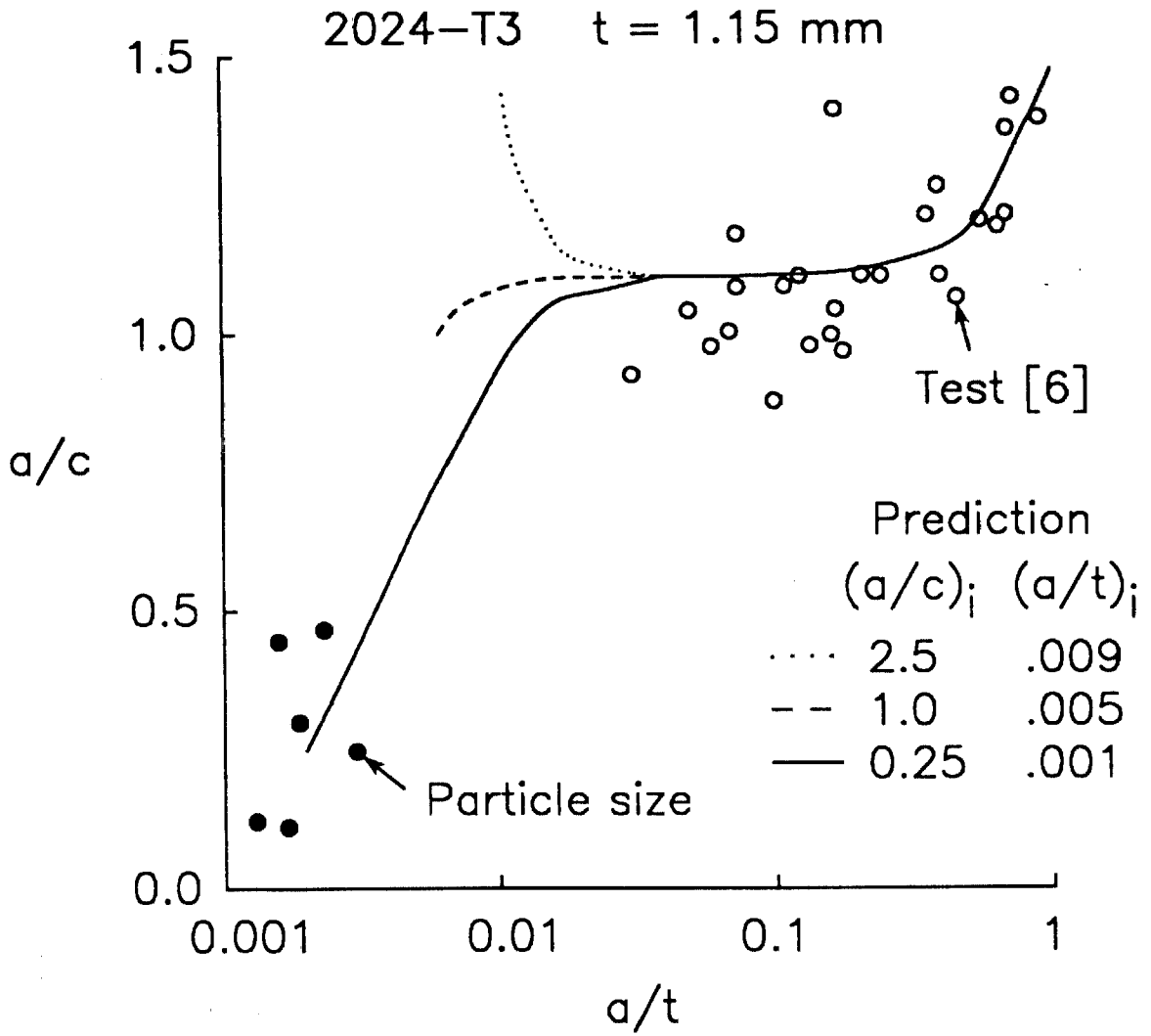

Figure 14.- Comparison of measured and predicted crack shape changes for small surface cracks at a notch in 2024-T3 aluminum alloy.

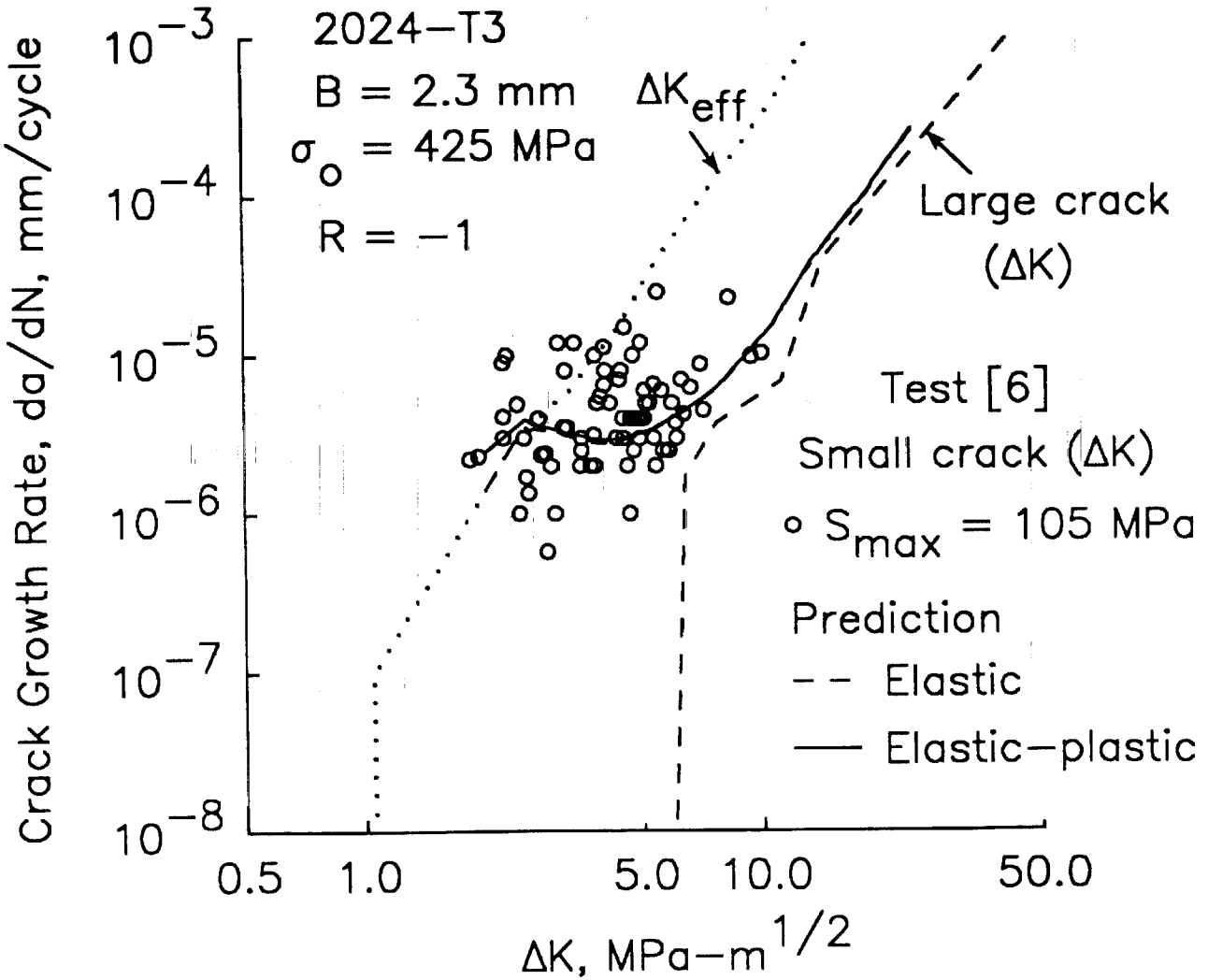

Figure 15.- Comparison of measured and predicted small-crack growth rates in SENT specimens made of 2024-T3 aluminum alloy.

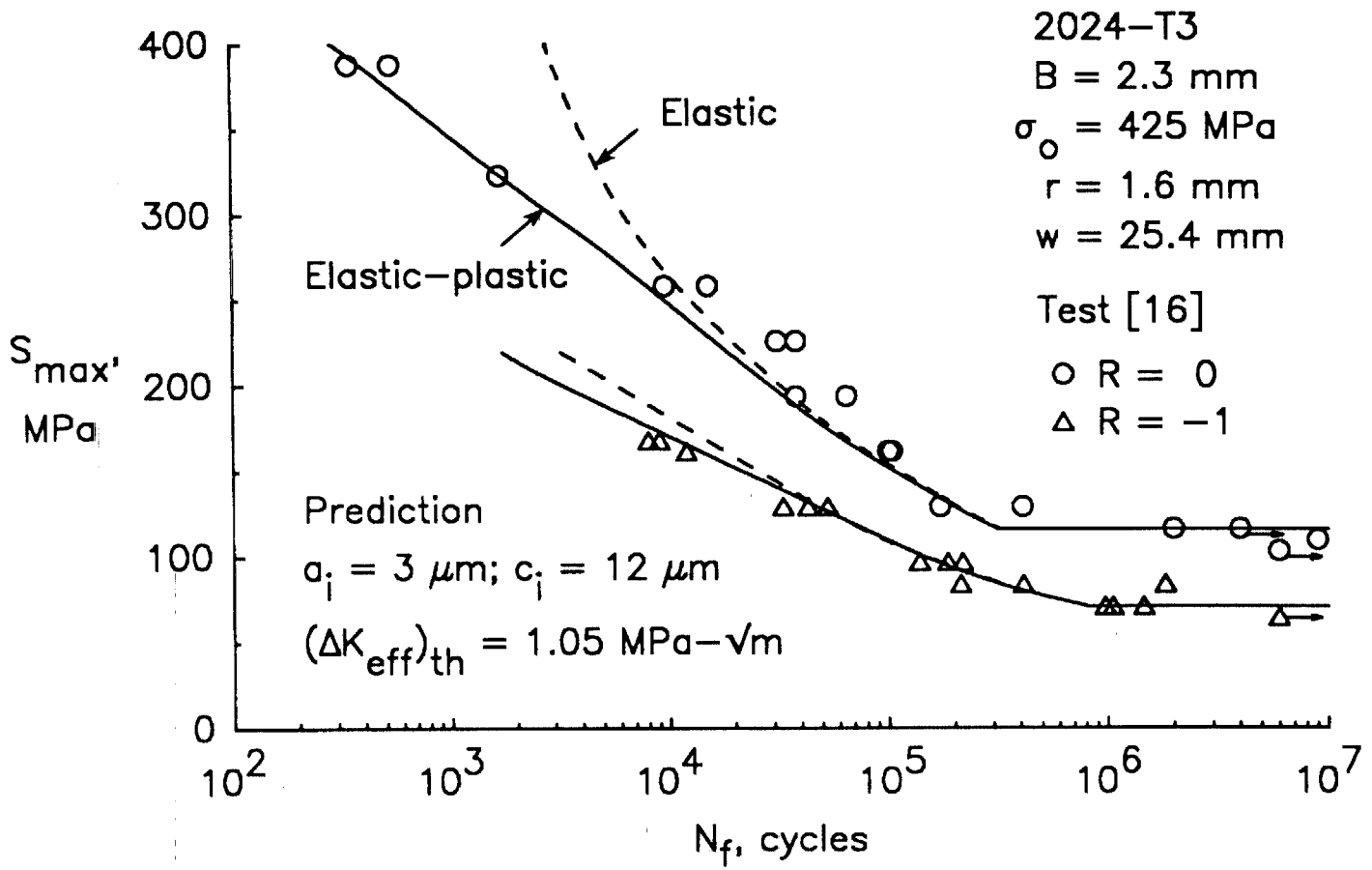

Figure 16.- Comparison of measured and predicted fatigue lives for 2024-T3 aluminum alloy sheet specimens with a circular hole.

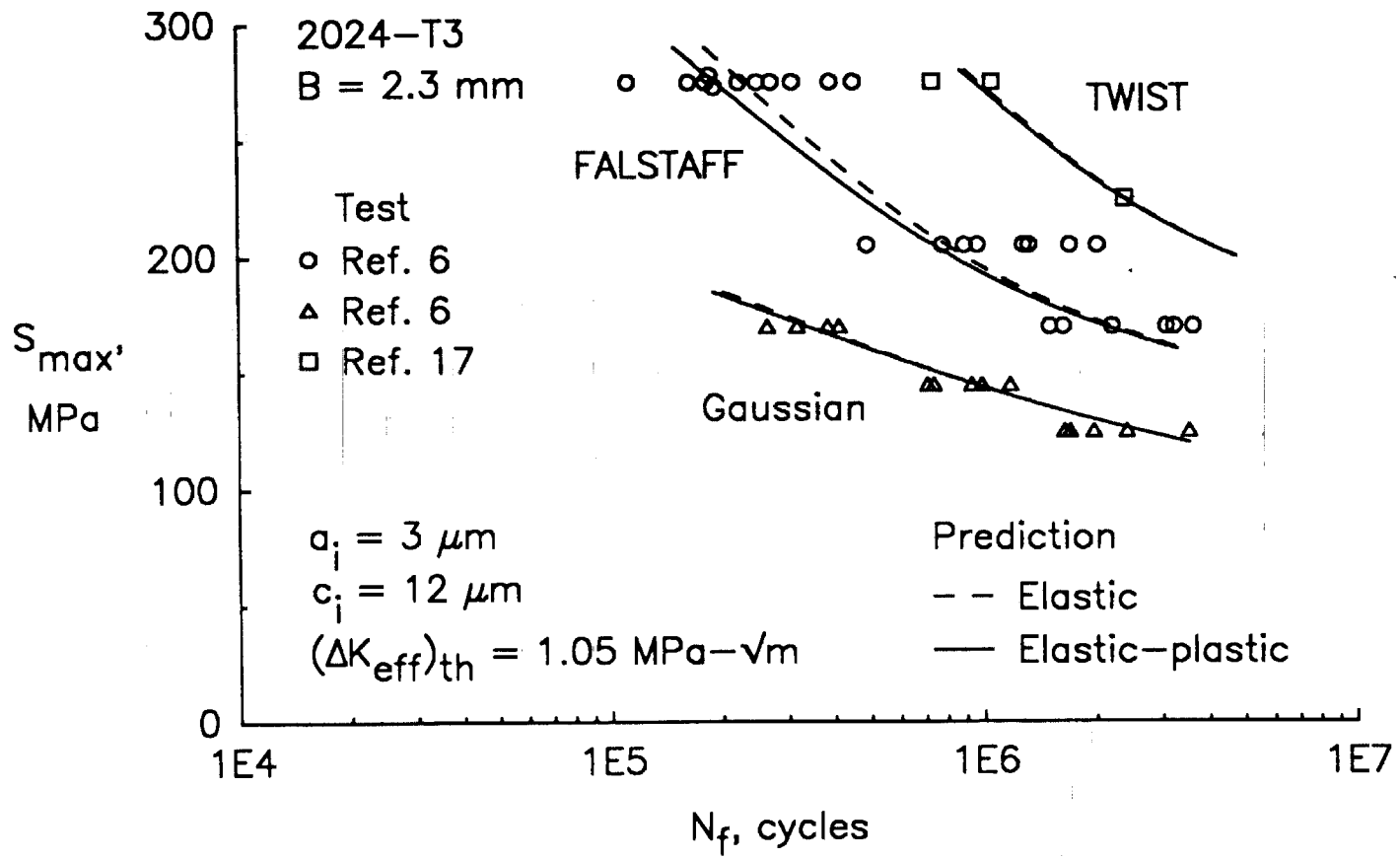

Figure 17.- Comparison of measured and predicted fatigue lives to breakthrough for SENT specimens under three spectrum loadings.

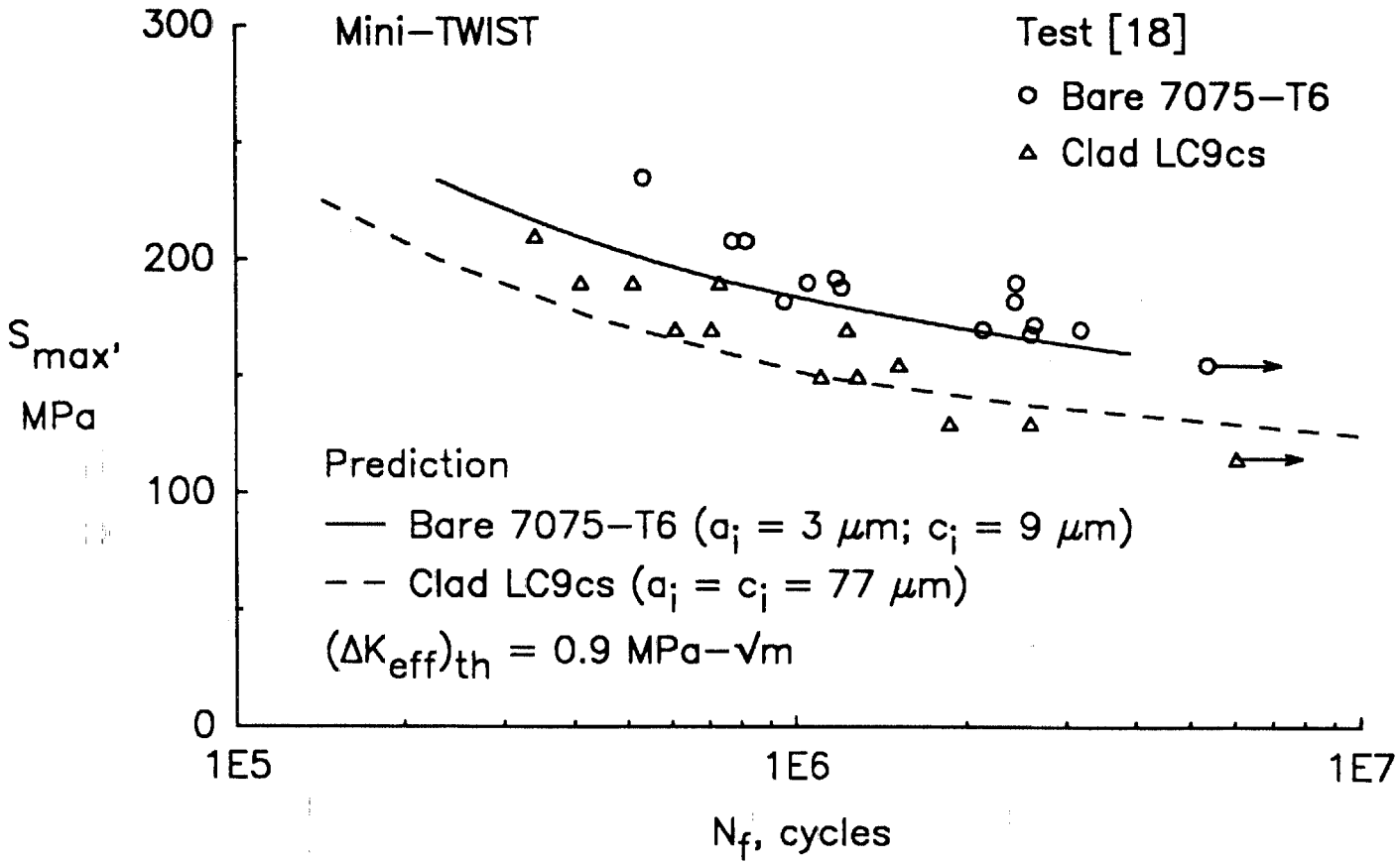

Figure 18.- Comparison of measured and predicted fatigue lives for SENT specimens made of bare and clad aluminum alloys under Mini-TWIST spectrum loading.

REPORT DOCUMENTATION PAGE

Form Approved
OMB No. 0704-0188

1. AGENCY USE ONLY *(Leave blank)*	2. REPORT DATE	3. REPORT TYPE AND DATES COVERED
	August 1992	Technical Memorandum

4. TITLE AND SUBTITLE
Advances in Fatigue Life Prediction Methodology for Metallic Materials

5. FUNDING NUMBERS
WU 505-63-50-04

6. AUTHOR(S)
J. C. Newman, Jr.

7. PERFORMING ORGANIZATION NAME(S) AND ADDRESS(ES)
NASA Langley Research Center
Hampton, VA 23681

8. PERFORMING ORGANIZATION REPORT NUMBER

9. SPONSORING / MONITORING AGENCY NAME(S) AND ADDRESS(ES)
National Aeronautics and Spac Administration
Washington, DC 20546-0001

10. SPONSORING / MONITORING AGENCY REPORT NUMBER
NASA TM-107676

11. SUPPLEMENTARY NOTES

12a. DISTRIBUTION / AVAILABILITY STATEMENT
Unclassified - Unlimited

Subject Category 39

12b. DISTRIBUTION CODE

13. ABSTRACT *(Maximum 200 words)*

The objective of this paper is to review capabilities of a plasticity-induced crack-closure model to predict small- and large-crack growth rates, and in some cases total fatigue life, for four aluminum alloys and three titanium alloys under constant-amplitude, variable-amplitude, and spectrum loading. Equations to calculate a cyclic-plastic-zone corrected effective stress-intensity factor range from a cyclic J-integral and crack-closure analysis of large cracks were reviewed. The effective stress-intensity factor range against crack growth rate relations were used in the closure model to predict small- and large-crack growth under variable-amplitude and spectrum loading. Using the closure model and microstructural features, a total fatigue life prediction method is demonstrated for three aluminum alloys under various load histories.

14. SUBJECT TERMS	15. NUMBER OF PAGES
Crack; Fatigue, Metals; Plasticity; Crack propagation; Small cracks	45
	16. PRICE CODE: A03

17. SECURITY CLASSIFICATION OF REPORT	18. SECURITY CLASSIFICATION OF THIS PAGE	19. SECURITY CLASSIFICATION OF ABSTRACT	20. LIMITATION OF ABSTRACT
Unclassified	Unclassified		